ATLAS CONF Note

ATLAS-CONF-2022-007

28th March 2022

Constraints on spin-0 dark matter mediators and invisible Higgs decays using ATLAS 13 TeV pp collision data with two top quarks and missing energy in the final state

The ATLAS Collaboration

This paper presents a statistical combination of searches targeting final states with two top quarks and invisible particles and characterised by the presence of zero, one or two leptons, at least one jet originating from a b-quark and missing transverse momentum. The analyses are performed with the ATLAS detector using 139 fb^{-1} of pp collisions at a centre-of-mass energy of 13 TeV at the LHC and search for phenomena beyond the Standard Model consistent with the production of dark matter particles at colliders. The results are interpreted in terms of simplified dark matter models with a spin-0 scalar or pseudoscalar mediator particle. In addition, the results are interpreted in terms of upper limits on the Higgs boson invisible branching ratio, where the Higgs boson is produced according to the Standard Model in association with a pair of top quarks. For scalar (pseudoscalar) dark matter models, the statistical combination extends the excluded mass range by 100 (30) GeV with respect to the best of the individual channels, excluding mediator masses up to 370 GeV for unitary couplings assumptions. In addition, the statistical combination improves the expected coupling exclusion reach by 14% (24%), assuming a scalar (pseudoscalar) mediator of 10 GeV. An upper limit on the Higgs boson invisible branching ratio of 0.40 ($0.30^{+0.13}_{-0.09}$) is observed (expected) at 95% confidence level.

ATLAS-CONF-2022-007
29 March 2022

1 Introduction

The existence of a non-luminous component of matter in the universe, dark matter (DM), is supported by compelling astrophysical evidence [1, 2]. Dark matter abundance has been accurately determined from global fits of cosmological parameters to a variety of observations [3, 4]. Nevertheless, the nature of DM remains largely unknown.

In this paper, models where the DM candidate is a weakly interactive massive particle (WIMP) [5] are considered. At the Large Hadron Collider (LHC), pair-produced WIMP DM does not interact with the ATLAS detector and it can be detected only if produced in association with Standard Model (SM) particles, leading to signatures with missing transverse momentum. A wide range of experimental searches are focused on WIMP candidates at the LHC [6–12]. All recent searches are based on simplified benchmark models documented in the LPCC Dark Matter Working Group whitepapers [13–16]. Benchmark models are chosen to have a minimal number of additional parameters with respect to the SM. This paper focuses on simplified models characterised by the introduction of a spin-0 particle mediator [15–23]. In this case, fermionic DM particle pairs are produced through the exchange of a colour-neutral scalar or pseudoscalar mediator (denoted by ϕ or a, respectively). Due to the Minimal Flavour Violation [24] assumption, the interaction between any new neutral spin-0 state and SM quarks is proportional to the fermion masses via Yukawa-type couplings and it is also treated as free parameter of the model by means of a multiplicative factor g_q. Following Ref. [23], couplings to leptons and W/Z bosons, as well as explicit $\phi - h$ or $a - h$ couplings of dimension four, are set to zero. The coupling of the mediator to the dark sector, g_χ, is not taken to be proportional to the mass of the DM candidates and treated simply as a free parameter. The dominant production modes for colour-neutral mediators are loop-induced gluon-fusion and associated production of the mediator with a top quark pair. The associated production of spin-0 mediators with a single top quark has also a sizeable, albeit non-dominant, cross section [19, 25, 26], especially for higher mediator masses. The primary signal of interest in this paper is the associated production of a mediator particle with a pair of top quarks (DM+$t\bar{t}$), although sensitivity is retained also in case of single top quark productions (collectively referred as DM+t). The relevant processes for DM+$t\bar{t}$ and DM+t are shown in Figure 1. The relative contribution of the two processes depends on the parameter space that is considered [25].

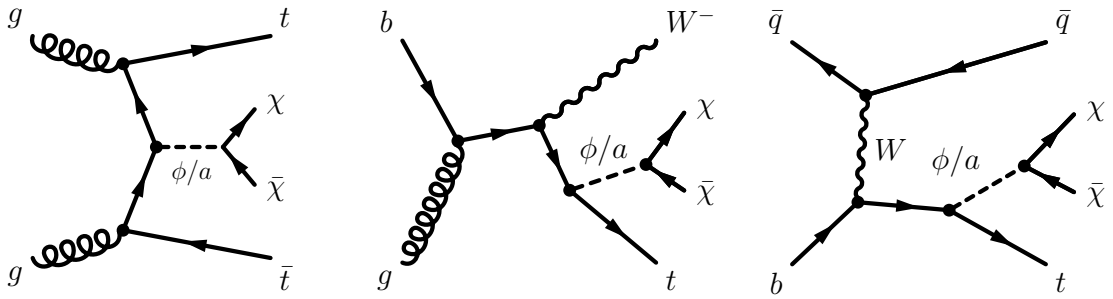

(a) (b) (c)

Figure 1: Representative diagrams for spin-0 mediator associated production with (a) a top quark pair (DM+$t\bar{t}$), (b) a single top quark and a W boson (DM+tW) or (c) a single top quark and one (or more) jet(s) (DM+tj).

This paper presents the statistical combination of three searches targeting events with two top quarks and invisible particles considering either zero- (tt0L [27]), one- (tt1L [28]) or two-lepton (tt2L [29]) final states,

using 139 fb^{-1} of pp collisions data recorded by the ATLAS detector [30] at a centre-of-mass energy of $\sqrt{s}$ = 13 TeV. The tt0L analysis is extended and improved with respect to Ref. [27] benefiting from the Run-2 improvements in the trigger selection of jets containing b-hadrons (b-jets) in ATLAS [31] that increases the sensitivity in models with light mediator masses. The three analyses select independent (orthogonal) datasets which can be statistically combined to boost the sensitivity as they constrain similar parts of the parameter space. Searches targeting specifically the associated production of a single top quark and invisible particles [32] are not orthogonal to the searches presented here. They are therefore not included and their combination is left as future development.

The data are found to be in agreement with the SM background prediction in all selections considered in this paper. The statistical combination is used to set 95% confidence level (CL) constraints to simplified DM models. The specific case where the mediator corresponds to the SM 125 GeV Higgs boson [33] is also considered to interpret the results presented in this paper. It is referred to as $H \to$ inv interpretation in the following. In the SM, the invisible Higgs boson branching ratio, $\mathcal{B}_{H\to\text{inv}}$, is 0.12% from $H \to ZZ \to 4\nu$ decays [34], and higher branching ratios to invisible particles are predicted by Higgs-dark matter portal models [35–48]. The strongest existing limits on invisible branching ratio are from the statistical combination of search results, for which ATLAS reported an observed (expected) limit of 0.26 (0.17) [49] and CMS reported 0.19 (0.15) [50] at 95% CL. Recent updates by the ATLAS and CMS Collaborations in the vector-boson-fusion channel report improved observed (expected) upper limits of 0.145 (0.103) [51] and 0.18 (0.10) [52], respectively, using the full Run-2 dataset.

The paper is structured as follows: the experimental dataset and the simulated event samples are presented in Section 2, the new and previously published searches are introduced in Section 3, their statistical combination, including the correlation treatment of systematic uncertainties is discussed in Section 4. Results in terms of exclusion limits are presented in Section 5. Finally, additional details of the extended 0-lepton channel are discussed in Appendix A.

2 Data and simulated event samples

The dataset used in the analyses described in this paper consists of pp collisions data recorded by the ATLAS detector [30] at a centre-of-mass energy of $\sqrt{s}$ = 13 TeV with stable beam conditions. The ATLAS detector is a multi-purpose particle detector with a forward-backward symmetric cylindrical geometry and nearly full coverage in solid angle[1] It consists of an inner tracking detector surrounded by a thin superconducting solenoid providing a 2 T axial magnetic field, electromagnetic and hadron calorimeters, and a muon spectrometer. An extensive software suite [53] is used in the reconstruction and analysis of real and simulated data, in detector operations, and in the trigger and data acquisition systems of the experiment. All collision events considered in this paper are required to have at least one reconstructed interaction vertex with a minimum of two associated tracks each having $p_{\text{T}} > 500$ MeV. In events with multiple vertices, the one with the highest sum of squared transverse momenta of associated tracks is chosen as the primary vertex [54]. Electrons [55], muons [56], τ [57] leptons and jets are reconstructed by combining the signals from the different components of the ATLAS detector. Small-radius jets are

[1] ATLAS uses a right-handed coordinate system with its origin at the nominal interaction point (IP) in the centre of the detector and the z-axis along the beam pipe. The x-axis points from the IP to the centre of the LHC ring, and the y-axis points upward. Cylindrical coordinates (r, ϕ) are used in the transverse plane, ϕ being the azimuthal angle around the z-axis. The pseudorapidity is defined in terms of the polar angle θ as $\eta = -\ln\tan(\theta/2)$. The angular distance between two objects in $\eta - \phi$ space is defined by $\Delta R \equiv \sqrt{(\Delta\eta)^2 + (\Delta\phi)^2}$.

reconstructed from energy deposits in the calorimeters using the anti-k_t jet algorithm [58, 59] and using a radius parameter of $R = 0.4$. Reclustered large-radius jets are reconstructed with the same algorithm using small-radius jets as inputs with a radius parameter of $R = 1.2$, unless otherwise specified. Multivariate algorithms are used to identify small-R jets with transverse momentum, p_{T} greater than 20 GeV containing b-hadrons (b-jets) [60, 61]. This is referred to as b-tagging. The missing transverse momentum $\boldsymbol{p}_{\mathrm{T}}^{\mathrm{miss}}$ (with magnitude $E_{\mathrm{T}}^{\mathrm{miss}}$) is calculated from the negative vector sum of transverse momenta of electrons, muons and jet candidates and an additional soft term [62] which includes activity in the tracking system originating from the primary vertex but not associated with any reconstructed object.

Depending on the analysis channel, events are selected by lepton triggers [63, 64], $E_{\mathrm{T}}^{\mathrm{miss}}$ triggers [65] or b-jet triggers [31]. The uncertainty in the combined integrated luminosity is 1.7% [66], obtained using the LUCID-2 detector [67] for the primary luminosity measurements. Events accepted by lepton and $E_{\mathrm{T}}^{\mathrm{miss}}$ triggers are required to meet the standard ATLAS data quality assessment criteria [68] to confirm the normal functionality of all standard sub-detector systems. This leads to the integrated luminosity of 3.2 fb^{-1}, 33.0 fb^{-1}, 44.3 fb^{-1} and 58.5 fb^{-1} in 2015, 2016, 2017 and 2018 data-taking, respectively, with a total luminosity of 139.0 fb^{-1}. Events accepted by b-jet triggers are required to meet additional criteria ensuring that the online beamspot position measurement is valid, which leads to the exclusion of the 2015 data and to the reduced integrated luminosity of 24.6 fb^{-1}, 43.7 fb^{-1} and 57.7 fb^{-1} in 2016, 2017 and 2018 data-taking, respectively, with a total luminosity of 126.0 fb^{-1}. The b-jet trigger chains considered in this paper require at least four jets, among which two jets b-tagged by the online version of the b-tagging boosted decision tree algorithm [61].

Dedicated Monte Carlo (MC) simulated samples are used to aid in the estimation of the background from SM processes and to model the dark matter signal. All simulated events are processed through an ATLAS detector simulation [69, 70]. The simulated events are reconstructed with the same algorithms as those used for data. They contain a realistic modelling of additional pp collisions in the same and nearby bunch crossings (pile-up), obtained by overlaying minimum-bias events simulated using the soft QCD processes of Pythia 8.186 [71, 72] with the NNPDF2.3 Leading Order (LO) set of parton distribution functions (PDFs) [73] and the A3 [74] set of tuned parameters.

Standard Model processes involving one or two top quarks in the final states are modelled using Powheg Box v2 [75–78] and normalised using Next-to-Next-to-Leading order (NNLO) plus Next-to-Next-to-Leading-Log (NNLL) [79] QCD accuracies. Processes involving the production of one (two) vector boson(s) are generated using Sherpa 2.2.1 [80–84] (2.2.2) and normalised at NNLO [85] (NLO) QCD cross section accuracy. Finally, $t\bar{t} + V$ ($V = W, Z, h$), tZ and tWZ processes are generated using MadGraph5_aMC@NLO [86] v2.3.3 and normalised at NLO QCD cross section accuracy [86, 87].

Signal samples for dark matter associated production with two top quarks (DM+$t\bar{t}$) are generated using a LO matrix element, with up to one extra parton using the MadGraph5_aMC@NLO [86] v2.6.7 generator interfaced to Pythia 8.244 and using the CKKW-L merging algorithm [88].

PDFs are provided by the five-flavour scheme NNPDF3.0 NLO [89] PDF set. The top quark decay is simulated using MadSpin [90]. Signal cross sections for this process are calculated to NLO QCD accuracy using the same version of MadGraph, as suggested in Ref. [91]. The typical scaling from LO to NLO of these calculations range between 1.25 and 1.35, depending on the mediator mass and whether it is a scalar or a pseudoscalar boson. Signal samples for dark matter associated production with a single top quark are generated using the same settings as the DM+$t\bar{t}$ samples. For these signal models the tW and the tj processes are generated separately. Each one is normalised to the LO cross section predicted by the

model and then the samples are combined (added together). No extra partons from the matrix element are generated in this case.

Signal samples modelling the 125 GeV Higgs invisible decays are generated using POWHEG BOX v2 [75–77, 92] generator at NLO with the NNPDF3.0NLO [89] PDF set. The Higgs boson decays via ZZ^* to neutrinos, and the signal samples are normalised using the total $t\bar{t}H$ cross section at NLO QCD and electroweak accuracy recommended by the LHC Higgs cross section working group [87]. Only the associated production of the Higgs boson with two top quarks is considered in the simulated samples. Rarer processes such as tH and tWH are neglected.

For the SM background samples, except those generated using SHERPA, the EVTGEN v1.2.0 [93] program is used to simulate the properties of the b- and c-hadron decays and PYTHIA 8.186 with the A14 tune [94] is used for the parton showering hadronisation model and underlying event. For the SHERPA generator, the default SHERPA [80–84] configuration recommended by the SHERPA authors is used. The modeling of the response of the various ATLAS subdetectors is performed using GEANT4 [70] for all the background MC samples, while all signal MC samples are simulated using a faster simulation based on a parameterisation of the calorimeter response and GEANT4 for the other detector systems [69].

3 Experimental signatures and analysis strategy

All analyses require the presence of at least one b-tagged jet and $E_{\mathrm{T}}^{\mathrm{miss}}$ in the event. To further suppress events where the $E_{\mathrm{T}}^{\mathrm{miss}}$ is originating from mismeasurements, the ratio of the $E_{\mathrm{T}}^{\mathrm{miss}}$ over its resolution is used to construct the missing momentum significance [95], $\mathcal{S}$, of the event.

The tt0L analysis targets decay chains with no leptons in the final state. This analysis is composed of a set of regions defined in order to obtain maximal significance for target-signal events (referred to as signal regions, SR) previously published in Ref. [27], dubbed tt0L-high, and uses the $E_{\mathrm{T}}^{\mathrm{miss}}$ triggers to select events with large missing transverse momentum and at least one highly energetic, hadronically decaying top quark candidate. An additional set of SRs, dubbed tt0L-low, is presented in this paper for the first time and extends the previously published results by relying on a combination of $E_{\mathrm{T}}^{\mathrm{miss}}$ and b-tagged jet triggers to retain events with objects with lower momentum that fail one of the tt0L-high analysis criteria.

The two other analyses considered in this paper target instead leptonic final states. The tt1L analysis [28] selects events with exactly one lepton (e or μ) and it is based on the $E_{\mathrm{T}}^{\mathrm{miss}}$ triggers. The tt2L analysis [29] targets events with exactly two opposite-charge leptons (e or μ) in the final states selected with dileptonic triggers.

Common event-quality criteria and object reconstruction and identification definitions for leptons, jets, b-tagged jets and $E_{\mathrm{T}}^{\mathrm{miss}}$ are applied in all analyses considered in the combination. The lepton multiplicity requirements guarantee that the 0-lepton, 1-lepton and 2-lepton channels are by construction non-overlapping due to the lepton multiplicity requirements. The specific reconstruction algorithms, working points and efficiencies can be found in Refs. [27–29] and in Appendix A. For all analyses in this paper, background-enriched selections (control regions, CR) are defined to aid in the estimation of the dominant SM backgrounds and validation regions (VR) are used to support the robustness of this estimate. A dedicated background estimation strategy has been developed for each channel [27–29], using independent control regions for all dominant SM processes.

Observed and expected number of events in the signal and control regions are used as Poisson probability functions to build a likelihood function and combined into a profile likelihood fit. A profile likelihood ratio statistics is employed to exclude at 95% CL the signal-plus-background hypothesis using the CL_s method for the considered signal models [96–99].

3.1 Description of analysis channels

The tt0L analysis The experimental signature targeted in this channel consists of at least four jets, two of which being b-tagged, and large missing transverse momentum ($E_{\mathrm{T}}^{\mathrm{miss}} > 160$ GeV). Events with electrons, muons or τ leptons are rejected. The tt0L-high selection consists of events with high missing transverse momentum ($E_{\mathrm{T}}^{\mathrm{miss}}$ trigger, $E_{\mathrm{T}}^{\mathrm{miss}} > 250$ GeV, $\mathcal{S} > 14$) where at least one of the jets reconstructed with large-radius has a mass consistent with having been produced from a hadronic top quark decay. This selection corresponds to signal region selections SRA and SRB in Ref. [27], which were originally optimised to be sensitive to high mass supersymmetric top squarks and are divided into three categories (TT, TW and T0), depending on whether the subleading large-radius jet has an invariant mass consistent with a top quark, a W boson or neither. Given the signature and kinematic similarity between the signal considered in this paper and top squark pairs decaying into a top and a neutralino, these regions can be also used to constrain DM+$t\bar{t}$ models. SRA and SRB are orthogonal thanks to a requirement on the χ^2-based stransverse mass variable, m_{T2,χ^2}, and statistically combined. This stransverse mass [100, 101] variable aims to reconstruct the mass of two heavy particles produced in an event and decaying symmetrically into an invisible particle and a top quark, as expected in supersymmetric top quark topologies. It relies on a χ^2-based method to identify the hadronically decaying top quark candidates. The background estimation of SRA and SRB is aided by means of dedicated control regions for all dominant SM processes: $t\bar{t}Z$, Z+jets, $t\bar{t}$, single top quark in the tW channel, and W+jets. Event yields with updated jet calibrations [102] were recalculated with respect to [27] and are presented in Figure 2(a). The yield change due to the new calibration is between 6% and 15% and is reflected on the signal predictions as well. This is due to the fact that the new calibration decreases the contribution of events with artificially increased missing transverse momentum due to mismeasured jets in the analysis by reducing the tails of the missing transverse momentum significance distribution. This translates to a slightly improved signal-over-background ratio in the tt0L-high SRs.

The tt0L-low selection is newly added in this paper with the aim to improve the sensitivity of the 0-lepton channel for dark matter models by selecting final states with lower missing transverse momentum and/or lower momentum objects. To this aim, events are therefore selected by a combination of $E_{\mathrm{T}}^{\mathrm{miss}}$ triggers and b-jet triggers. Events selected with $E_{\mathrm{T}}^{\mathrm{miss}}$ triggers must fulfil $E_{\mathrm{T}}^{\mathrm{miss}} > 250$ GeV to ensure the triggers are fully efficient. In addition, they are required to have either $\mathcal{S} < 14$ or no large-radius jets consistent with highly energetic top quark candidates to ensure orthogonality with the tt0L-high selections. Events selected with b-jet triggers must fulfil the requirement on missing transverse momentum to be between 160 and 250 GeV. The lower bound suppresses the multi-jets background contamination, while the upper bound ensures orthogonality with tt0L-high. The online b-tagged jet candidates must match the offline b-tagged jet candidates within a cone of $\Delta R = 0.2$.

The tt0L-low selection is designed to maximise the sensitivity to DM+$t\bar{t}$ signals with low mediator masses ($m(\phi), m(a) < 100$ GeV). Three signal regions are defined, SR0X, SRWX and SRTX, according to the mass of the large-radius jet with highest mass, which is used to infer the p_{T} of the most energetic top quark in the event. SR0X requires the presence of no large-radius jets (0), while in SRWX and SRTX the mass of the highest mass large-radius jet has to be respectively lower and higher than 130 GeV, i.e.

in the neighbourhood of the W boson (W) or the top quark (T) mass. A smaller radius parameter of $R = 1.0$ in the jet reconstruction procedure with respect to the tt0L-high channel, associated to newly introduced lower selections on the large-radius jet transverse momentum ($p_{\mathrm{T}} > 200$ GeV) and invariant mass ($m_{\text{large-radius jet}} > 40$ GeV), are found to increase the separation between signal and background in the phase space considered in the tt0L-low channel[2]. Less energetic final states are targeted in the tt0L-low analysis compared to the tt0L-high analysis, such that the decay products of the top quarks are expected to be less collimated. Hence no subleading large-radius jet is required (X).

The full list of requirements for the three tt0L-low signal regions is reported in Table 1. Angular separation variables are used to reduce the contamination from multi-jet events ($\Delta\phi_{\mathrm{min}}(\boldsymbol{p}_{\mathrm{T,1\text{-}4}}, \boldsymbol{p}_{\mathrm{T}}^{\mathrm{miss}})$), to reduce the contamination from b-jets from gluon splitting as present in Z+jets events ($\Delta R\left(b_1, b_2\right)$), and to enhance the fraction of events with hadronic top quarks such as in the signal (ΔR_{min}(large-radius jet, b-tagged jets)). The SM background originating from the top quark is reduced using the $\cosh_{\mathrm{max}}$ variable (Appendix A). This variable aims to identify events where a leptonically decaying W boson is the source of the entire $E_{\mathrm{T}}^{\mathrm{miss}}$ in the event. It is defined as the maximal value of the hyperbolic cosine of the pseudorapidity difference between the missed W boson and each of the two b-tagged jets selected in the event (b_1 and b_2):

$$\cosh_{\mathrm{max}} = \max\{\cosh(\eta_W - \eta_{b_1}), \cosh(\eta_W - \eta_{b_2})\}. \tag{1}$$

The unknown value of the W boson pseudorapidity, η_W, is estimated by solving the kinematic of the top quark decay while assuming that, given the $E_{\mathrm{T}}^{\mathrm{miss}}$ requirement, $m_W \ll p_{\mathrm{T}}^W \cdot \cosh\eta_W$. Events with high $\cosh_{\mathrm{max}}$ values are likely to contain a top quark decaying leptonically and excluded from the signal regions. In addition, a χ^2-based variable, $\chi^2_{t\bar{t},\,\mathrm{had}}$, is used to identify events with a hadronically decaying top quark pair as present in the signal (Appendix A). The $\chi^2_{t\bar{t},\,\mathrm{had}}$ variable is constructed using up to six jets in the event and using the b-tagging classification when appropriate to reconstruct the two W bosons and the two top quarks in the event. Invariant mass constraints terms for all these particles are used to build the χ^2. The event distributions for the $\cosh_{\mathrm{max}}$ and the $\chi^2_{t\bar{t},\,\mathrm{had}}$ variables after applying all SR0X selection requirements except those on the quantity presented in each distribution are shown in Figure 3. Furthermore, the transverse momentum of the $t\bar{t}$ system ($p_{\mathrm{T}}^{t\bar{t}}$) constructed with the $\chi^2_{t\bar{t},\,\mathrm{had}}$ method is compared to the $E_{\mathrm{T}}^{\mathrm{miss}}$. In signal events these two quantities are expected to have similar values, hence, events with $p_{\mathrm{T}}^{t\bar{t}}/E_{\mathrm{T}}^{\mathrm{miss}}$ values outside a window centred to unity are excluded to reject further background events.

The main contribution to the SM background in the signal regions originates from single top quark events in the tW channel and $t\bar{t}$ events, with a lepton missed by the reconstruction algorithms, and $Z \to \nu\nu$ events (Z+jets, $t\bar{t}+Z$). Contrary to the tt0L-high SRs, $t\bar{t}$ is the dominant contribution in the tt0L-low selections, due to the lower $E_{\mathrm{T}}^{\mathrm{miss}}$ requirements. Dedicated control regions are used to aid the background estimation of the signal regions for all dominant processes and follow a similar approach to the tt0L-high analysis for single top quark in the tW channel, Z+jets and $t\bar{t}+Z$. No W+jets control regions are defined since it represents less than 5% of the total background across all three tt0L-low signal regions. Due to the importance of the $t\bar{t}$ background in the tt0L-low selections, $t\bar{t}$ events with extra b-hadrons ($t\bar{t}+b$) are treated separately from $t\bar{t}$ events without extra jets or events with extra light flavour jets (referred to as *other*) in the tt0L-low analysis, and distinct control regions for each of the two components are defined. This is justified by the fact that $t\bar{t}$+b events are more likely to pass the signal region selections than $t\bar{t}$ (other) events due to the presence of extra b-jets which makes it more difficult to isolate and reconstruct the $t\bar{t}$ system. In practice, this results in a significant shape difference in the $\cosh_{\mathrm{max}}$ variable between $t\bar{t}$

[2] To ensure orthogonality between the two analyses, the selection on large-radius jets based on the definition used in the tt0L-high analysis ($R = 1.2$) is used for vetoing the events.

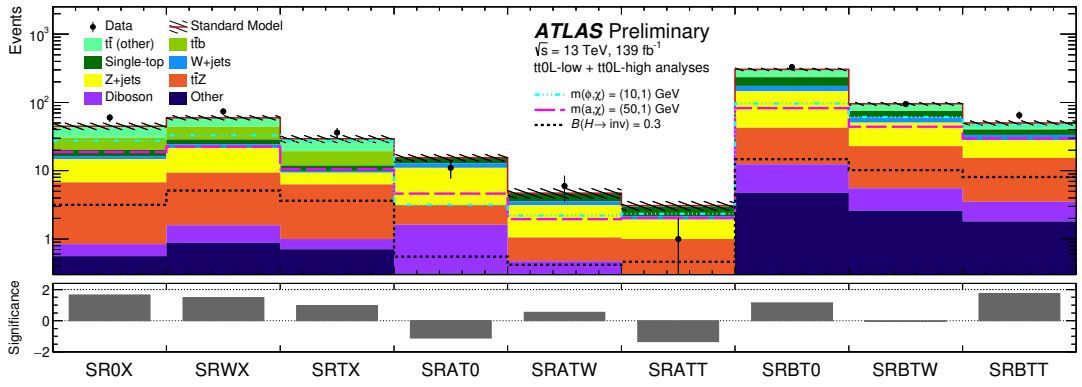

(a)

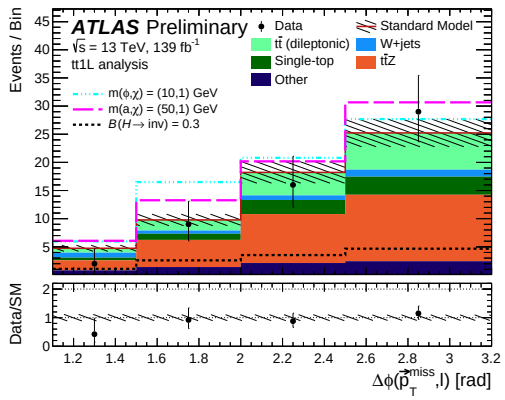

(b)

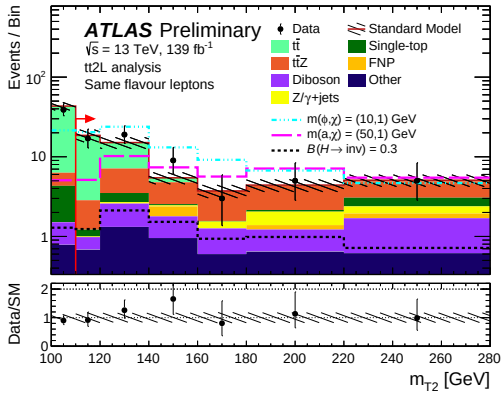

(c)

Figure 2: (a) Final signal region yields for the tt0L-high and the tt0L-low analyses. The bottom panel shows the statistical significance [103] of the difference between the SM prediction and the observed data in each region. The definition of SRAT0, SRATW, SRATT, SRBT0, SRBTW and SRBTT can be found in Ref. [27]. Representative post-fit distributions are presented for (b) the tt1L and (c) the tt2L analyses: each bin of such distributions, starting from the red arrow in (c), corresponds to a single SR included in the fit. In the tt0L-low analysis, '$t\bar{t}$ (other)' represents $t\bar{t}$ events without extra jets or events with extra light flavour jets. In the tt2L analysis, 'FNP' includes contribution from fake/non-prompt lepton background arising from jets (mainly π/K, heavy flavour hadron decays and photon conversion) misidentified as leptons, estimated in a pure data-driven way. 'Other' includes contributions from $t\bar{t}+W$, tZ and tWZ processes, and additionally $t\bar{t}$ (semi-leptonic) for the tt1L analysis. The total uncertainty on the SM expectation is represented with hashed bands and the expected distributions for selected signal models are also shown as dashed lines.

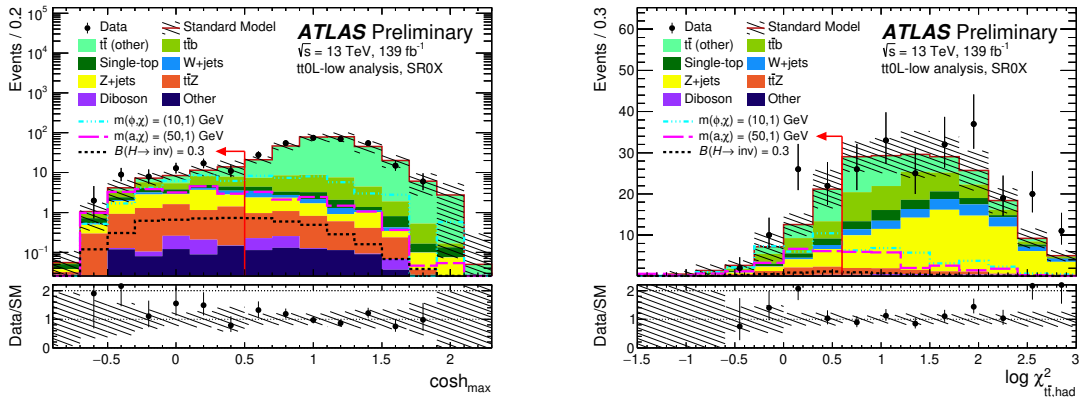

(a) (b)

Figure 3: (a) $\cosh_{\text{max}}$ and (b) $\chi^2_{t\bar{t},\,\text{had}}$ distributions in SR0X passing all the SR requirements except those on the variable being presented (which are indicated by the arrows). The contributions from all SM backgrounds are shown after the profile likelihood simultaneous fit to all tt0L-low CRs, with the hashed bands representing the total uncertainty. '$t\bar{t}$ (other)' represents $t\bar{t}$ events without extra jets or events with extra light flavour jets. 'Other' includes contributions from $t\bar{t}+W$, tZ and tWZ processes. The expected distributions for selected signal models are also shown as dashed lines. The underflow (overflow) events are covered in the first (last) bin. The bottom panels show the ratio of the observed data to the total SM background prediction, with the hatched area representing the total uncertainty in the background prediction.

Table 1: Selection criteria for the signal regions used in the tt0L-low analysis.

Variables	**SR0X**	**SRWX**	**SRTX**
N_{lepton}	$= 0$		
Orthogonalisation	$E_{\text{T}}^{\text{miss}} < 250$ GeV or $\mathcal{S} < 14$ or $m^{R=1.2}_{\text{large-radius jet}} < 120$ GeV		
$E_{\text{T}}^{\text{miss}}$ [GeV]	> 160 < 250, when passing b-jet triggers		
$\mathcal{S}$	> 10		
$\Delta\phi_{\text{min}}(\boldsymbol{p}_{\text{T,1-4}}, \boldsymbol{p}_{\text{T}}^{\text{miss}})$	> 1.0	> 0.5	
$\Delta R\,(b_1, b_2)$	> 1.2		
$N_{\text{large-radius jet}}$	$= 0$	> 0	
$m_{\text{large-radius jet}}$ [GeV]	—	(40, 130)	≥ 130
ΔR_{min}(large-radius jet, b-tagged jets)	—		< 1.2
$\cosh_{\text{max}}$	< 0.5	< 0.6	< 0.7
$\chi^2_{t\bar{t},\,\text{had}}$	< 4	< 6	< 8
$p_{\text{T}}^{t\bar{t}}/E_{\text{T}}^{\text{miss}}$	(0.7, 1.2)	(0.5, 1.2)	

(other) and $t\bar{t}+b$ events. Moreover, a larger simulation mismodelling for the $t\bar{t}+b$ events with respect to $t\bar{t}$ (other) events is observed and can be corrected by splitting the two components.

The background estimates are validated in dedicated, non-overlapping, validation regions, which require no lepton, while being orthogonal to the signal region selections. In such regions, the background prediction agrees with the data within 1 σ. More details are given in Appendix A.

The expected number of events is estimated using a profile likelihood simultaneous fit to all tt0L-low CRs and is presented in Table 2. The observed data is compatible within two sigma with the prediction.

The results presented in this paper show the final tt0L combination between the tt0L-low and the tt0L-high. The details of this combination and the single-channel individual limits are discussed Appendix A.

Table 2: Expected and observed numbers of events in SR0X, SRWX and SRTX. The background yields and uncertainties are shown after the profile likelihood simultaneous fit to all tt0L-low CRs. '$t\bar{t}$ (other)' represents $t\bar{t}$ events without extra jets or events with extra light flavour jets. 'Other' includes contributions from $t\bar{t}+W$, tZ and tWZ processes. The quoted background uncertainties include both the statistical and systematic contributions, while the signal uncertainties are purely statistical.

Process	**SR0X**	**SRWX**	**SRTX**
Observed data	60	74	36
Expected SM events	45 ± 8	59 ± 6	28 ± 5
$t\bar{t}$ (other)	14 ± 4	15 ± 4	9.4 ± 3.5
$t\bar{t}+b$	10 ± 7	15.0 ± 3.1	7.2 ± 2.8
Single-top	3.8 ± 3.0	4.3 ± 2.6	1.9 ± 1.5
Z+jets	8.0 ± 1.6	12.1 ± 2.3	3.1 ± 0.8
W+jets	1.6 ± 1.1	2.7 ± 2.1	0.6 ± 0.6
$t\bar{t}+Z$	5.9 ± 1.0	7.8 ± 1.3	5.3 ± 1.1
Diboson	0.28 ± 0.20	0.7 ± 0.4	0.30 ± 0.19
Other	0.55 ± 0.15	0.88 ± 0.24	0.70 ± 0.22
Pre-fit $t\bar{t}$	15	17	9.8
Pre-fit $t\bar{t}+b$	7	11.5	5.6
Pre-fit Single-top	7.1	8.2	3.6
Pre-fit Z+jets	6.1	9.2	2.3
Pre-fit $t\bar{t}+Z$	5.9	7.9	5.4
Benchmark signal models			
DM $m(\phi,\chi)=(10,1)$ GeV	27.4 ± 2.4	33.2 ± 2.2	27.5 ± 2.2
DM $m(a,\chi)=(50,1)$ GeV	18.8 ± 1.3	22.6 ± 1.5	10.6 ± 1.0
$H\rightarrow$ inv ($\mathcal{B}$ =100%)	10.52 ± 0.34	17.1 ± 0.4	12.1 ± 0.4

The tt1L analysis This analysis requires exactly one lepton (e or μ), at least four jets, two of which must be b-tagged, and $E_{\mathrm{T}}^{\mathrm{miss}} > 230$ GeV, and was specifically designed to target spin-0 DM models. The $\mathcal{S}$ is required to be above 15 and, only for this analysis, it is defined only considering jets and leptons in the events and their resolution, as described in Ref. [104]. A recursive reclustering jet algorithm with variable radius [105] is used to identify at least one large-variable-radius jet loosely consistent with a top quark ($m_{\mathrm{top}^{\mathrm{reclustered}}} > 150$ GeV). The use of a variable-radius algorithm instead of a fixed one helps increasing the acceptance of both highly boosted and less boosted events when no explicit categorisation is performed, as

in this analysis. In addition, a requirement on the topness likelihood variable [106] selects events which are not consistent with the dileptonic decay of the SM $t\bar{t}$ process. $E_{\mathrm{T}}^{\mathrm{miss}}$ triggers were used to select data that then populates this SR. This region is further split into four disjoint regions according to the azimuthal distance between the $E_{\mathrm{T}}^{\mathrm{miss}}$ and the lepton momentum, $\Delta\phi(\boldsymbol{p}_{\mathrm{T}}^{\mathrm{miss}}, \ell)$, which are presented in Figure 2(b). An additional requirement of $\Delta\phi(\boldsymbol{p}_{\mathrm{T}}^{\mathrm{miss}}, \ell) > 1.1$ is applied. The dominant backgrounds, $t\bar{t}$ and $t\bar{t}Z$, are estimated by means of dedicated CRs.

The tt2L analysis The last analysis considers events with two opposite-charge leptons (e or μ), at least one b-tagged jet and significant $E_{\mathrm{T}}^{\mathrm{miss}}$ ($\mathcal{S} > 12$), exploiting events collected with dileptonic triggers. Events are then split depending on whether the two leptons have the same or different flavour, and in the same-flavour selection the additional requirement of $|m_{\ell\ell} - m_Z| > 20$ GeV is added to suppress the Z+jets background. In this selection, the main discriminating variable is the leptonic stransverse mass m_{T2} [100, 101], which is used to bound the individual masses of a pair of particles that are each presumed to have decayed into one visible and one invisible particle. This quantitiy is used to bound dileptonic top pair decays. To maximise the search sensitivity, the m_{T2} spectrum is divided into six bins, starting from 110 GeV. The m_{T2} distribution for events selected with two leptons with the same flavour is presented in Figure 2(c). In this search, the main backgrounds are $t\bar{t}$, $t\bar{t}Z$, single top quark in the tW channel, Z+jets, and diboson processes. Those backgrounds are estimated with MC simulations, constrained with data in orthogonal CRs for the dominant contributions ($t\bar{t}$ and $t\bar{t}Z$), while the background arising from fake/non-prompt leptons (FNP) is estimated in a pure data-driven way.

3.2 Orthogonalisation

In order to combine the results of the different searches, those are requested to be statistically independent and any possible overlap in term of kinematic regions have been investigated and removed. All analysis channels are disjoint thanks to the requirement on the lepton multiplicity. The tt0L-high and tt0L-low channels are kept orthogonal by the requirements on the large-radius jet as well as on the $E_{\mathrm{T}}^{\mathrm{miss}}$ and the $\mathcal{S}$. In addition, one of the Z+jets CRs in the tt0L-high analysis, denoted as CRZAB-T0 in Ref. [27], is not considered and a single control region, CRZAB-TTTW, is used to normalise the Z+jets process in all SRs of the tt0L-high analysis. This has a negligible impact on the tt0L-high analysis results and it is done to ensure orthogonality between the Z+jets CRs of the tt0L-high and tt0L-low analyses. To the same end, the Z+jets CR of the tt0L-low analysis only selects events either with $\mathrm{N}_{\text{large-radius jet}} < 2$ or with the subleading large-radius jet mass < 60 GeV.

An overlap is present in the definition of the CRs for the constrain of the $t\bar{t}Z$ background. For this process, the analyses adopted a similar strategy and constrained the $t\bar{t}Z$ (with $Z \to \nu\nu$) populating their SRs with events with three leptons where the purity of $t\bar{t}Z$ (with $Z \to \ell\ell$) is maximised. Such regions differ only by minor selections adapted to the SR of each specific channel. In the combination, the $t\bar{t}Z$ estimation is harmonised by using the most inclusive $\mathrm{CR}_{t\bar{t}Z}$ from the tt2L analysis [29] as common CR across all channels. The fitted normalisation parameter obtained in the combination is consistent with the one published in Ref [28] within 1%.

4 Statistical combination and uncertainties

The statistical combination of the analyses considered in this paper consists of maximising a profile likelihood ratio [97] constructed from the product of the individual analyses likelihoods:

$$\Lambda(\alpha;\theta) = \frac{L\left(\alpha, \hat{\hat{\theta}}(\alpha)\right)}{L\left(\hat{\alpha}, \hat{\theta}\right)}.$$

The α and θ parameters represent respectively the parameter of interest and the nuisance parameters. In the numerator, the nuisance parameters are set to their profiled values $\hat{\hat{\theta}}(\alpha)$, which maximise the likelihood function for fixed values of the parameter of interest α. In the denominator, both the parameter of interest and the nuisance parameters are set to the values that jointly maximise the likelihood: $\hat{\alpha}$ and $\hat{\theta}$, respectively.

For the DM signal model interpretations, upper limits on the signal cross section are provided following the CL_s formalism using the profile likelihood ratio as a test statistic. The overall signal strength, defined as a scale factor multiplying the cross section predicted by the signal hypothesis, is the parameter of interest and it is bounded from below at zero. The final result is provided in terms of ratio between the lowest excluded signal cross section and the predicted cross section for unitary couplings. For the $H \to$ inv signal model interpretation, the $\mathcal{B}_{H\to\text{inv}}$ is consider as parameter of interest α, following the implementation described in Ref. [107, 108].

As described in Section 3, for each channel the estimation of the dominant SM backgrounds is aided by means of dedicated control regions that constrain free floating normalisation factors for each of these backgrounds.

Systematic uncertainties are modelled in the likelihood function as nuisance parameters θ constrained by Gaussian or log-normal probability density functions [109].

Three sources of systematic uncertainties are considered: detector-related (experimental) uncertainties, uncertainties related to the modelling of SM background processes and uncertainties related to the modelling of the signal processes. Regarding the experimental and SM modelling uncertainties, all details are given in Refs. [27–29], respectively for the zero-, one- and two-lepton channels. The tt0L-low channel considers the same uncertainties as the tt0L-high one and, in addition, uncertainties associated to the b-jet triggers efficiency. The typical size of these uncertainties is a few percent. All analyses use common event-quality criteria and object reconstruction and identification definitions. For this reason, all experimental systematic uncertainties are treated as correlated across channels in the statistical combination. The dominant sources of experimental systematic uncertainties in the combination are the uncertainties related to the jet energy and resolution, followed either by flavour tagging uncertainties or uncertainties related to the missing transverse momentum, depending on the analysis channel.

Uncertainties in the modelling of the SM background processes in MC simulation and their theoretical cross section uncertainties are also taken into account. All modelling uncertainties are treated as uncorrelated across different channels as they probe different corners of the available phase space.

Uncertainties related to the MC modelling of the DM signals include fragmentation and renormalisation scales, and the uncertainties related to the modelling of the parton shower. The impact of these uncertainties varies from 10% up to 25%. Uncertainties related to the $t\bar{t}H$ with $H \to$ inv signal modelling also include

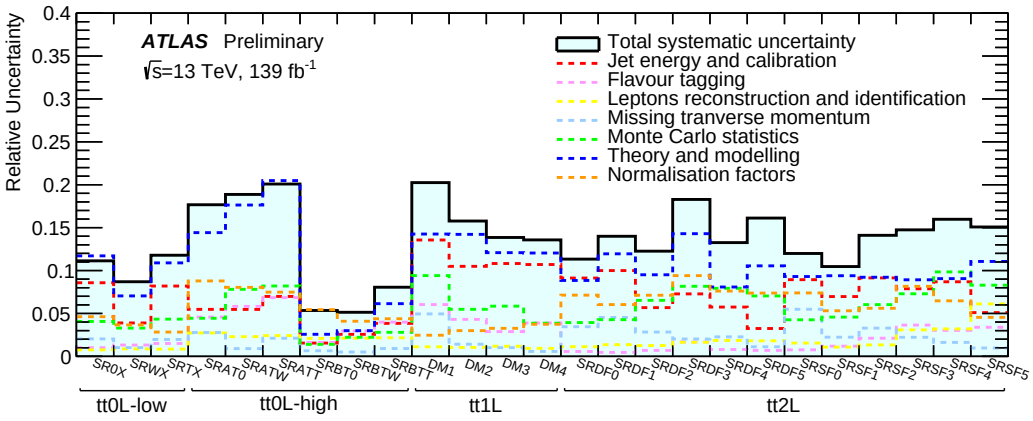

Figure 4: Summary of the total uncertainties on the background predictions of each SR of the tt0L-low, tt0L-high, tt1L, tt2L analysis channels in the statistical combination. Their dominant contributions are also indicated by individual lines. Individual uncertainties can be correlated, and do not necessarily add up in quadrature to the total background uncertainty.

fragmentation and renormalisation scale uncertainties, parton shower uncertainties and PDF uncertainties. Among these, scale uncertainties, which are evaluated with a particular focus on the impact on the simplified template cross sections formalism [34], are the dominant contribution and range between 7% to 17%. Signal modelling uncertainties are treated as fully correlated across analysis channels.

All sources of uncertainties on the SM backgrounds are visually summarised in Figure 4. In most of the SRs, the dominant systematic uncertainties are the ones related to theory predictions and MC modelling, while jet uncertainties are dominating between the experimental ones. No significant difference is observed in either the composition or the value of the total uncertainty presented in the published individual analyses.

5 Exclusion limits

Exclusion limits at 95% CL are presented in Figure 5(a) and 5(b) for DM models with a spin-0 scalar or pseudoscalar mediator particle, respectively. The three individual channels are also presented for comparison. The tt0L limits are the result of the statistical combination of the tt0L-low and tt0L-high SRs. The tt0L-low selection improves the expected scalar (pseudoscalar) mediator standalone cross section limit of the tt0L-high by up to 15% (5%) and it is strongest for mediator masses values around 10 GeV. Details of the comparison can be found in Appendix A.3.

The signal generation considered in these results includes both top quark pair final states (DM+$t\bar{t}$) and single top quark final states (DM+tW and DM+tj). The limits are expressed in terms of the ratio of the excluded cross section to the nominal cross section for a coupling assumption of $g = g_q = g_\chi = 1$. Under these assumptions, scalar DM models are characterised by a higher cross section with respect to pseudoscalar DM models at low mediator masses [20], while the two models have very similar cross sections beyond the top decay threshold ($m(\phi)/m(a) \sim 2 \cdot m_t$). A DM particle mass of 1 GeV is considered, although the results are valid as long as the mass of the mediator is larger than twice the mass of the DM. The solid (dashed) lines show the observed (expected) exclusion limits for each individual analysis and their statistical combination. For scalar (pseudoscalar) DM models, the combination extends the excluded mass

range by 100 (30) GeV with respect to the best of the individual analyses, excluding mediator masses up to 370 GeV. In addition, the combination improves the expected cross section limit by 14% and 24%, for low mass scalar and pseudoscalar DM mediators, respectively. This directly converts into more stringent excluded couplings. When only the associated production of DM and two top quarks is considered in the interpretation of the results, the excluded scalar (pseudoscalar) mediator mass range obtained from the combination is reduced by 70 (20) GeV with respect to the sensitivity of the combination as reported in Figures 5(a) and 5(b). As the associated production of DM and single top quark processes mostly contributes for higher masses in the scalar mediator models [25], the impact of this process for masses below 50 GeV is negligible. For the pseudoscalar mediator models, the ratio between the single top quark channel and the $t\bar{t}$ channel cross sections is instead relatively constant [25]. When considering only the $t\bar{t}$ plus DM associated production, the cross section upper limit is worsened by about 18% throughout the whole mass range.

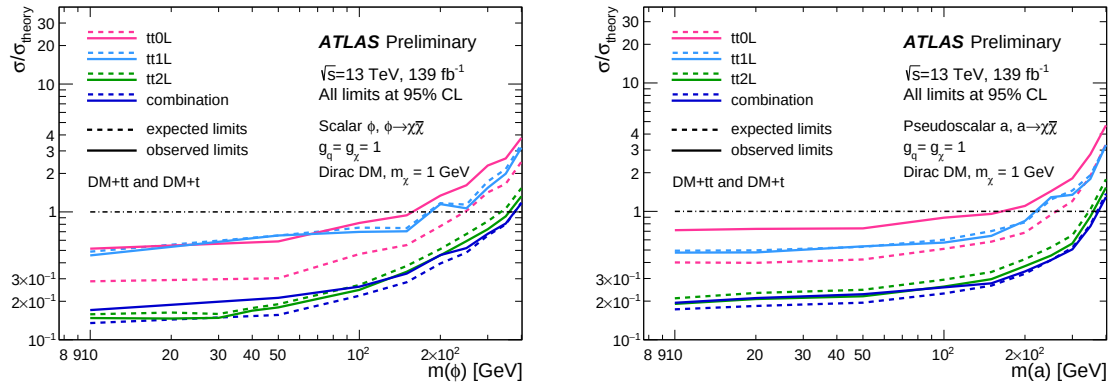

(a) (b)

Figure 5: Exclusion limits for colour-neutral (a) scalar or (b) pseudoscalar mediator dark matter models as a function of the mediator mass $m(\phi)$ or $m(a)$ for a DM mass $m_\chi = 1$ GeV. Associated production of DM with both single top quarks (tW and tj channels) and top quark pairs are considered. The limits are calculated at 95% CL and are expressed in terms of the ratio of the excluded cross section to the nominal cross section for a coupling assumption of $g = g_q = g_\chi = 1$. The solid (dashed) lines show the observed (expected) exclusion limits for each individual channel and their statistical combination.

The negative logarithmic profile likelihood ratios $-2\,\Delta\ln(\Lambda)(\mathcal{B}_{H\to\text{inv}};\theta)$ as a function of $\mathcal{B}_{H\to\text{inv}}$ of the individual analyses and of their combination are shown in Figure 6. Expected results are obtained using the Asimov dataset technique [97]. The best-fit values of $\mathcal{B}_{H\to\text{inv}}$ for the individual analyses are compatible within one standard deviation. Their statistical combination yields a best-fit value of $0.08^{+0.16}_{-0.15}$, consistent with the SM prediction of 0.12%. The combined observed 95% CL upper limit on $\mathcal{B}_{H\to\text{inv}}$ is 0.40 while the expected value is $0.30^{+0.13}_{-0.09}$. The individual analysis results are presented in Table 3, while the details of the tt0L combination are reported in Appendix A.3. The overall uncertainty is dominated by the limited statistics of the data and, to a smaller extent, by systematic uncertainties associated with the modelling of the SM processes and jet-related uncertainties. The Higgs boson invisible decays represent a specific case of the DM simplified models considered in the previous section, where the mass of the scalar mediator is assumed to be 125 GeV. The two results are consistent with each other, when taking into account the different accuracy used for the generation of the $H \to$ inv model.

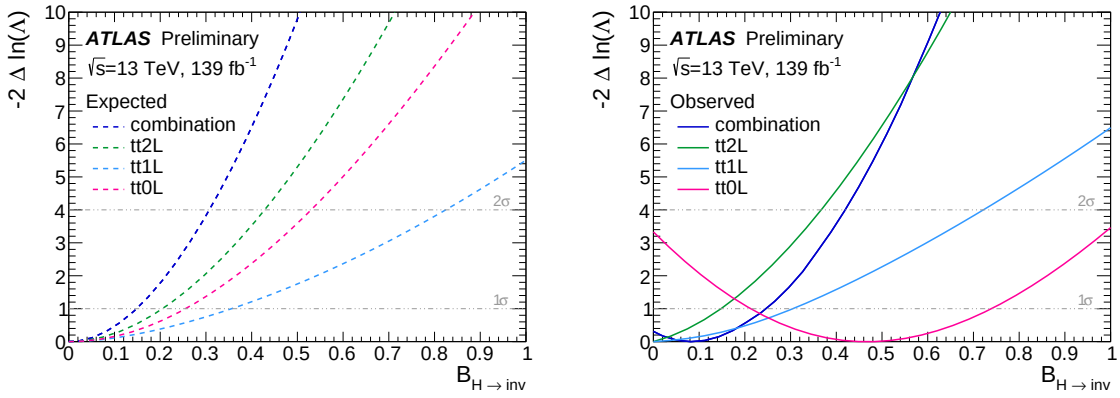

(a) (b)

Figure 6: (a) The expected negative logarithmic profile likelihood ratios $-2\,\Delta\ln(\Lambda)$ as a function of $\mathcal{B}_{H\to\text{inv}}$ for the each of the three channels and their statistical combination. (b) Shown are the same distributions for the observed curves.

Table 3: Summary of results from direct searches for invisible decays of the 125 GeV Higgs boson in the $t\bar{t}H$ topology using 139 fb^{-1} of Run 2 data, and their statistical combination. Shown are the best-fit values of $\mathcal{B}_{H\to\text{inv}}$, computed considering the parameter of interest not bounded at zero, for consistency with previous results [109]. Observed and expected upper limits on $\mathcal{B}_{H\to\text{inv}}$ at the 95% CL are computed with the CL_s method and are a new result with respect to the individual analysis papers quoted in the last table column. The corresponding Asimov datasets for the expected results are constructed using nuisance parameter values from a fit to data with $\mathcal{B}_{H\to\text{inv}} = 0$, and the quoted uncertainty corresponds to the 68% confidence interval.

Analysis	Best fit $\mathcal{B}_{H\to\text{inv}}$	Observed upper limit	Expected upper limit	Reference
tt0L	$0.48^{+0.27}_{-0.27}$	0.95	$0.52^{+0.23}_{-0.16}$	[27], this document
tt1L	$-0.04^{+0.35}_{-0.29}$	0.74	$0.80^{+0.40}_{-0.26}$	[28], this document
tt2L	$-0.09^{+0.22}_{-0.20}$	0.39	$0.42^{+0.18}_{-0.12}$	[29], this document
$t\bar{t}H$ comb.	$0.08^{+0.16}_{-0.15}$	0.40	$0.30^{+0.13}_{-0.09}$	This document

6 Conclusion

In summary, a statistical combination of three analyses using 139 fb^{-1} of pp collisions delivered by the LHC at a centre-of-mass energy of 13 TeV and collected by the ATLAS detector has been presented. The three analyses all select events with two top quarks and invisible particles and consider all possible light lepton multiplicities arising from the decays of the two top quarks.

The statistical combination is used to set 95% confidence level constraints to spin-0 simplified dark matter models. All production modes with top quarks in the final state (DM+$t\bar{t}$, DM+t) are considered. For scalar (pseudoscalar) dark matter models, the combination extends the excluded mass range by 100 (30) GeV

with respect to the best of the individual channels, excluding mediator masses up to 370 GeV for unitary couplings assumptions. In addition, the combination improves the observed coupling exclusion limit by 24%, assuming a pseudoscalar mediator of 10 GeV.

The specific case where the mediator corresponds to the SM 125 GeV Higgs boson is also considered to interpret the results presented in this paper. An upper limit on the Higgs boson invisible branching ratio of 0.40 ($0.30^{+0.13}_{-0.09}$) is observed (expected) at 95% confidence level.

Appendix

A The tt0L-low analysis

The tt0L-low analysis aims to enhance the sensitivity to DM+$t\bar{t}$ signals with low mediator masses ($m(\phi), m(a) < 100$ GeV). Two main discriminating variables, $\cosh_{\text{max}}$ and $\chi^2_{t\bar{t},\,\text{had}}$, are defined to reduce the most dominant top quark backgrounds. Angular separations between b-tagged jets, $E_{\text{T}}^{\text{miss}}$ or large-radius jets are used to further reduce the contamination from the Standard Model processes. To ensure orthogonality with the tt0L-high selections, additional orthogonalisation requirements are also applied, as detailed in Section 3.1.

A.1 Discriminating variables

The full event selections performed in the signal regions can be found in Table 1. The discriminating variables are described in more detail below.

$\cosh_{\text{max}}$

The $\cosh_{\text{max}}$ variable is designed to discriminate signal events against single-top events in the tW channel and $t\bar{t}$ events with a lepton missed by the reconstruction algorithms (top with lost lepton), which are among the main backgrounds in the analysis. Such events may enter the signal regions due to high $E_{\text{T}}^{\text{miss}}$ originating from the $t \to bW \to bl\nu$ decay, and the lost lepton.

The reconstruction of events containing a top quark with a lost lepton is attempted under the assumption that $E_{\text{T}}^{\text{miss}}$ is equal to the p_{T} of the leptonically decaying W boson with lost lepton, $E_{\text{T}}^{\text{miss}} \sim p_{\text{T}}^{W}$.

The top with lost lepton can then be reconstructed by combining the missing transverse momentum with the correct b-tagged jet ($t \to bW$). In practice, a four-vector with p_{T} and ϕ corresponding to the $\boldsymbol{p}_{\text{T}}^{\text{miss}}$ vector and its mass equal to the W boson mass is built, while its pseudo-rapidity η_W (or equivalently p_z^W) remains unknown. Choosing the x-axis to be in the direction of p_{T}^{W} and adopting (E, p_x, p_y, p_z) coordinates:

$$\boldsymbol{p}_W = \left(\sqrt{(p_{\text{T}}^W)^2 + (p_z^W)^2 + m_W^2}, p_{\text{T}}^W, 0, p_z^W\right), \tag{2}$$

$$\boldsymbol{p}_b = \left(\sqrt{(p_{\text{T}}^b)^2 + (p_z^b)^2 + m_b^2}, p_{\text{T}}^b \cdot \cos(\phi_W - \phi_b), p_{\text{T}}^b \cdot \sin(\phi_W - \phi_b), p_z^b\right), \tag{3}$$

$$m_t^2 = (\boldsymbol{p}_W + \boldsymbol{p}_b)^2, \tag{4}$$

where the b superscript and subscript refer to one of the selected b-tagged jet. Replacing Equations (2) and (3) in (4), and assuming the massless limit for the b-tagged jet, the equivalence below is formed:

$$\sqrt{1+\left(\frac{m_W}{p_{\mathrm{T}}^W \cdot \cosh\eta_W}\right)^2} \cdot \cosh\eta_W \cdot \cosh\eta_b - \sinh\eta_W \cdot \sinh\eta_b = \frac{m_t^2 - m_W^2}{2p_{\mathrm{T}}^W p_{\mathrm{T}}^b} + \cos(\phi_W - \phi_b), \quad (5)$$

where η_W is unknown. Given that $E_{\mathrm{T}}^{\mathrm{miss}} \sim p_{\mathrm{T}}^W > 160$ GeV in the signal regions and $\cosh\eta_W \geq 1$, one can assume $m_W \sim 80$ GeV $\ll p_{\mathrm{T}}^W \cdot \cosh\eta_W$, such that:

$$\sqrt{1+\left(\frac{m_W}{p_{\mathrm{T}}^W \cdot \cosh\eta_W}\right)^2} \sim 1. \quad (6)$$

Equation (5) can be thus simplified:

$$\begin{aligned}\cosh(\eta_W - \eta_b) &\sim \frac{m_t^2 - m_W^2}{2p_{\mathrm{T}}^W p_{\mathrm{T}}^b} + \cos(\phi_W - \phi_b) \\ &\sim \frac{m_t^2 - m_W^2}{2E_{\mathrm{T}}^{\mathrm{miss}} p_{\mathrm{T}}^b} + \cos(\phi_{E_{\mathrm{T}}^{\mathrm{miss}}} - \phi_b).\end{aligned} \quad (7)$$

By definition, $\cosh(x) \geq 1$ so that one expects the right part of Equation (7) to be larger than 1 in case of a successful leptonic top reconstruction. Therefore, the discriminating observable $\cosh_{\mathrm{max}}$ is finally defined as:

$$\cosh_{\mathrm{max}} = \max\{\cosh(\eta_W - \eta_{b_1}), \cosh(\eta_W - \eta_{b_2})\}, \quad (8)$$

where b_1 and b_2 represent the leading two b-tagged jets selected in the event. Events with high $\cosh_{\mathrm{max}}$ values are likely to contain a top quark with lost lepton and excluded from the signal regions.

Figure 7 illustrates the modelling of the shape of $\cosh_{\mathrm{max}}$ in SRWX and SRTX. The $\cosh_{\mathrm{max}}$ distribution in SR0X is shown in Figure 3.

$\chi^2_{t\bar{t},\,\mathrm{had}}$

The $\chi^2_{t\bar{t},\,\mathrm{had}}$ observable attempts to quantify how likely an event is to include two hadronically decaying top quarks. It is therefore used primarily to reject backgrounds containing no hadronic top quarks, such as Z+jets events. It is defined as follows:

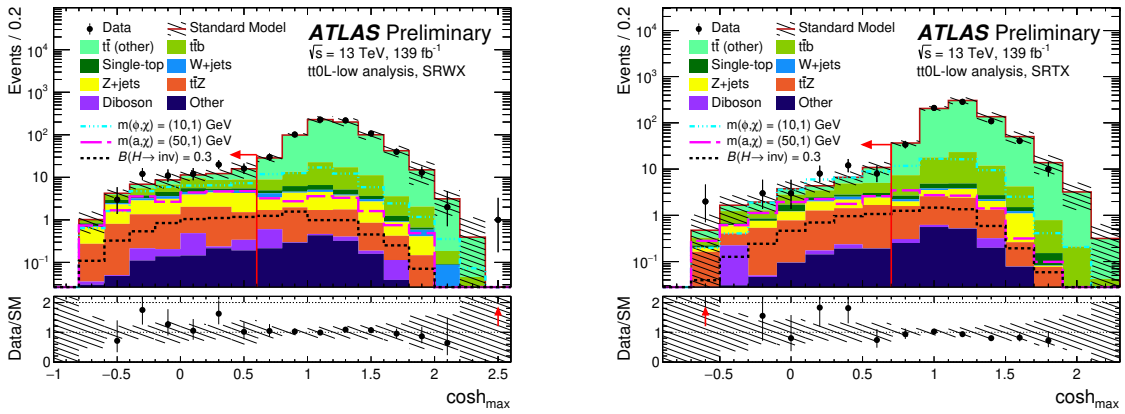

(a) (b)

Figure 7: $\cosh_{\text{max}}$ distributions in (a) SRWX and (b) SRTX passing all the SR requirements except those on $\cosh_{\text{max}}$ itself (which are indicated by the arrows). The contributions from all SM backgrounds are shown after the profile likelihood simultaneous fit to all tt0L-low CRs, with the hashed bands representing the total uncertainty. '$t\bar{t}$ (other)' represents $t\bar{t}$ events without extra jets or events with extra light flavour jets. 'Other' includes contributions from $t\bar{t}+W$, tZ and tWZ processes. The expected distributions for selected signal models are also shown as dashed lines. The underflow (overflow) events are covered in the first (last) bin. The bottom panels show the ratio of the observed data to the total SM background prediction, with the hatched area representing the total uncertainty in the background prediction and the red arrows marking data outside the vertical-axis range.

$$\chi^2_{t\bar{t},\,\text{had}} = \left(\frac{m_{W_1} - m_{W_{\text{ref}}}}{\sigma_{m_W}}\right)^2 + \left(\frac{(m_{t_1} - m_{W_1}) - (m_{t_{\text{ref}}} - m_{W_{\text{ref}}})}{\sigma_{m_t - m_W}}\right)^2 + \left(\frac{(m_{t_2} - m_{W_2}) - (m_{t_{\text{ref}}} - m_{W_{\text{ref}}})}{\sigma_{m_t - m_W}}\right)^2 . \tag{9}$$

Up to seven jets, including the two selected b-tagged jets, are considered in the calculation. The first W boson candidate, W_1, is built from two non b-tagged jets, while the first top quark candidate, t_1, combines W_1 and one of the b-tagged jets, b_1, such that $t_1 \to W_1 b_1$. According to Monte Carlo simulations, the second W boson candidate, W_2, is in more than 50% of the cases too soft to lead to two individual jets passing reconstruction criteria. Hence it is built from a single non b-tagged jet to which the mass of W boson is attributed. As a result, the second top quark candidate, $t_2 \to W_2 b_2$, contains only one non b-tagged and the remaining b-tagged jet b_2.

The first term in Equation (9) corresponds to the invariant mass constraint from W_1. The values $m_{W_{\text{ref}}}$ and σ_{m_W} are respectively the mean and the standard deviation of the experimental invariant mass distribution expected for hadronically decaying W bosons. The second and third terms correspond to the invariant mass constraints from t_1 and t_2. As m_{W_1} and m_{t_1} (m_{W_2} and m_{t_2}) are strongly correlated, the W boson is subtracted from the top mass to decouple these two terms from the first one. The values $m_{t_{\text{ref}}}$ and $\sigma_{m_t - m_W}$

are respectively the mean of the experimental invariant top mass distribution, and the standard deviation of the $m_t - m_W$ distribution expected for reconstructed hadronic top quarks. The values of $m_{W_{\text{ref}}}$, σ_{m_W}, $m_{t_{\text{ref}}}$ and $\sigma_{m_t - m_W}$ are taken from [110]:

- $m_{W_{\text{ref}}} = 80.51$ GeV, $\sigma_{m_W} = 12.07$ GeV,
- $m_{t_{\text{ref}}} - m_{W_{\text{ref}}} = 85.17$ GeV, $\sigma_{m_t - m_W} = 16.05$ GeV.

The χ^2 is recomputed for each possible jet combinations and the final $\chi^2_{t\bar{t},\,\text{had}}$ corresponds to the minimum value obtained. Events with high $\chi^2_{t\bar{t},\,\text{had}}$ values are less likely to contain two hadronic tops and therefore excluded from the signal regions.

Figure 8 illustrates the modelling of the shape of $\chi^2_{t\bar{t},\,\text{had}}$ in SRWX and SRTX. The $\chi^2_{t\bar{t},\,\text{had}}$ distribution in SR0X is shown in Figure 3.

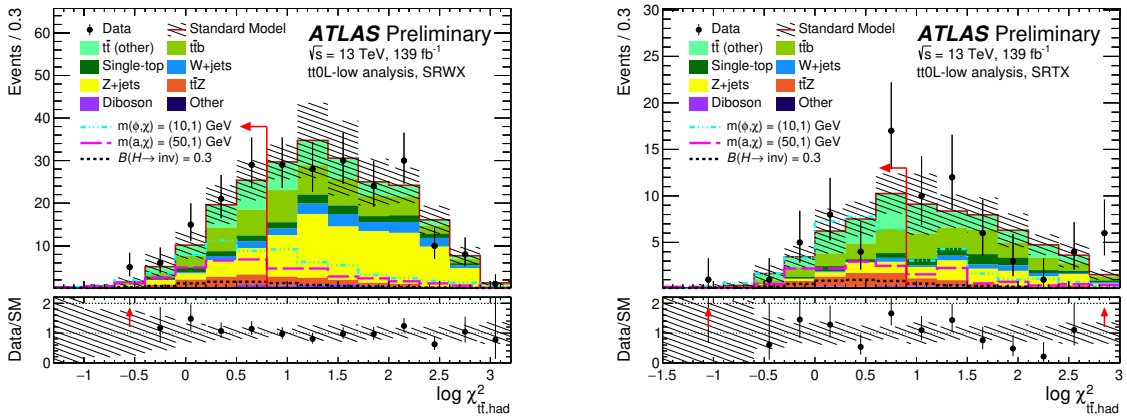

(a) (b)

Figure 8: $\chi^2_{t\bar{t},\,\text{had}}$ distributions in (a) SRWX and (b) SRTX passing all the SR requirements except those on $\chi^2_{t\bar{t},\,\text{had}}$ itself (which are indicated by the arrows). The contributions from all SM backgrounds are shown after the profile likelihood simultaneous fit to all tt0L-low CRs, with the hashed bands representing the total uncertainty. '$t\bar{t}$ (other)' represents $t\bar{t}$ events without extra jets or events with extra light flavour jets. 'Other' includes contributions from $t\bar{t}+W$, tZ and tWZ processes. The expected distributions for selected signal models are also shown as dashed lines. The underflow (overflow) events are covered in the first (last) bin. The bottom panels show the ratio of the observed data to the total SM background prediction, with the hatched area representing the total uncertainty in the background prediction and the red arrows marking data outside the vertical-axis range.

A.2 Background estimation

The event topologies in the signal and the control regions are kept as similar as possible to reduce any bias originating from differences in the kinematic phase space. For this purpose, control regions with lepton(s) in the final state are divided according to the mass of the large-radius jet with highest mass, as it is done for the signal regions, while all $E_{\text{T}}^{\text{miss}}$ related variables are recalculated by treating the selected leptons as invisible, denoted by the subscript 'no lepton' in the variable names.

One of the most prominent sources of backgrounds in the signals regions is the semi-leptonic $t\bar{t}$ decay where the lepton is misreconstructed or out of detector acceptance, while the contribution from the dileptonic

$t\bar{t}$ decay is negligible. Control regions selecting events with exactly one lepton (e or μ) are defined to estimate the background originating from a top quark decay with a lost lepton, which includes single-top events in the tW channel, $t\bar{t}+b$ and $t\bar{t}$ (other) events.

A χ^2 based observable [111], $\chi^2_{t\bar{t},\,\text{lep}}$, taking into account the kinematic properties of $E_{\text{T}}^{\text{miss}}$, lepton, jets and the b-tagging information, is used to reconstruct semi-leptonic $t\bar{t}$ events and separate them from tW and $t\bar{t}+b$ events. It follows a similar approach than the $\chi^2_{t\bar{t},\,\text{had}}$ variables by putting constraints on the masses of the hadronically decaying W boson, the hadronically decaying top quark and the leptonically decaying top quark. The presence of extra b-tagged jets is used to select $t\bar{t}+b$ over single-top processes. Tighter $\cosh_{\text{max, no lepton}}$ selections are required in the single-top control regions to reduce the contamination from semi-leptonic $t\bar{t}$ events failing the $\chi^2_{t\bar{t},\,\text{lep}}$ reconstruction and reach a high purity in tW events. Table 4 presents the full event selections applied to define the top with lost lepton control regions.

Table 4: Selection criteria for the top with lost lepton control regions used in the tt0L-low analysis.

	Variables	**CR0X**	**CRWX**	**CRTX**
shared selections	N_{lepton}	= 1		
	$E_{\text{T, no lepton}}^{\text{miss}}$ [GeV]	> 160		
	$E_{\text{T}}^{\text{miss}}$ [GeV]	< 250, when passing b-jet triggers		
	$\mathcal{S}_{\text{no lepton}}$	> 10		
	$\Delta\phi_{\text{min}}(\boldsymbol{p}_{\text{T,1-4}}, \boldsymbol{p}_{\text{T,no lepton}}^{\text{miss}})$	> 1.0	> 0.5	
	$\Delta R\,(b_1, b_2)$	> 1.2		
	$N_{\text{large-radius jet}}$	= 0	> 0	
	$m_{\text{large-radius jet}}$ [GeV]	—	(40, 130)	≥ 130
	ΔR_{min}(large-radius jet, b-tagged jets)	—		< 1.2
	$\cosh_{\text{max, no lepton}}$	< 0.9	< 0.95	< 1.0
	$\chi^2_{t\bar{t},\,\text{had}}$	< 10	< 20	< 40
	$p_{\text{T}}^{t\bar{t}}/E_{\text{T, no lepton}}^{\text{miss}}$	(0.7, 1.2)	(0.5, 1.2)	
$t\bar{t}$ (other) enriched selections	**Variables**	**CR0X**$_{t\bar{t}}$	**CRWX**$_{t\bar{t}}$	**CRTX**$_{t\bar{t}}$
	$\chi^2_{t\bar{t},\,\text{lep}}$	< 6		
$t\bar{t}+b$ enriched selections	**Variables**	**CR0X**$_{t\bar{t}+b}$	**CRWX**$_{t\bar{t}+b}$	**CRTX**$_{t\bar{t}+b}$
	$\chi^2_{t\bar{t},\,\text{lep}}$	≥ 6		
	$N_{\text{extra } b\text{-tagged jet}}$	≥ 1		
single-top enriched selections	**Variables**	**CR0X**$_{\text{single-top}}$	**CRWX**$_{\text{single-top}}$	**CRTX**$_{\text{single-top}}$
	$\chi^2_{t\bar{t},\,\text{lep}}$	≥ 30		
	$N_{\text{extra } b\text{-tagged jet}}$	= 0		
	$\cosh_{\text{max, no lepton}}$	< 0.5	< 0.6	< 0.7

Another major background component in the signal regions contains $Z \to \nu\nu$ produced in association to jets. Control regions selecting events with two leptons with opposite charge and same flavour (ee or $\mu\mu$) are defined to estimate the $Z(\nu\nu)$+jets background. The invariant mass and transverse momentum of the dilepton system, m_{ll} and p_{T}^{ll} respectively, and the missing transverse momentum significance $\mathcal{S}$ serve as the major discriminants to suppress the contamination from dileptonic $t\bar{t}$ events. Several selections applied in the signal regions are not considered to ensure sufficient statistics in the CRs. Table 5 presents the full event selections applied to define the Z+jets control regions.

Validation regions are not included in the statistical model and only serve to validate the extrapolation over

Table 5: Selection criteria for the Z+jets control regions used in the tt0L-low analysis.

Variables	**CR0X**$_{Z+\text{jets}}$	**CRWX**$_{Z+\text{jets}}$	**CRTX**$_{Z+\text{jets}}$
N_{lepton}	$= 2$		
Orthogonalisation	$N^{R=1.2}_{\text{large-radius jet}} < 2$ or $m^{R=1.2}_{\text{subleading large-radius jet}} < 60$ GeV		
$E^{\text{miss}}_{\text{T, no lepton}}$ [GeV]	> 160		
$\mathcal{S}_{\text{no lepton}}$	> 8		
$\Delta\phi_{\text{min}}(\boldsymbol{p}_{\text{T,1-4}}, \boldsymbol{p}^{\text{miss}}_{\text{T}})$	> 0.5		
$N_{\text{large-radius jet}}$	$= 0$	> 0	
$m_{\text{large-radius jet}}$ [GeV]	—	(40, 130)	≥ 130
m_{ll} [GeV]	(80, 100)		
p^{ll}_{T} [GeV]	> 160		
$\mathcal{S}$	< 5		

the lepton multiplicity when going from the control to the signal regions. The event selections performed in the validation regions therefore require no lepton, while being orthogonal to the signal region selections.

In the $t\bar{t}$-enriched validation regions, $t\bar{t}$ events are selected by inverting the tight $\cosh_{\text{max}}$ requirement applied in the signal regions and adding a looser upper threshold. The validation regions for $t\bar{t} + b$, single-top and Z+jets are merged into single $t\bar{t}$-suppressed validations regions due to the limited number of events in the 0-lepton phase space. In these regions the $\chi^2_{t\bar{t},\,\text{had}}$ selection applied in the signal regions is inverted. The $p^{t\bar{t}}_{\text{T}}/E^{\text{miss}}_{\text{T}}$ requirements are discarded as they become irrelevant when the value of $\chi^2_{t\bar{t},\,\text{had}}$ is too large. Tight $\Delta R\,(b_1, b_2)$ selections are required to minimise the contamination from W+jets events, with their thresholds optimised in each region to provide a similar number of events with respect to the $t\bar{t}$ enriched VRs. All the background predictions in the VRs agree with the data within 1σ.

A.3 Results

All tt0L-low signal and control regions are included in a statistical model based on the combined likelihood fit. The normalisation of the $t\bar{t}+b$, $t\bar{t}$ (other), single-top and Z+jets background processes are free-floating. For the $t\bar{t}$ background, the normalisation factors are decorrelated in the three kinematic regimes (CR0X, CRWX and CRTX) to account for a possible top quark p_{T} dependence of the normalisation factor. The yield results have been presented in Table 2.

Figure 9 shows the $E^{\text{miss}}_{\text{T}}$ distributions in the three tt0L-low signal regions. The background contributions are obtained from the profile likelihood simultaneous fit to all tt0L-low CRs with a background-only hypothesis.

Exclusion limits at 95% CL are presented in Figure 10(a) and 10(b) for DM models with a spin-0 scalar or pseudoscalar mediator particle, respectively. The tt0L-low analysis, the tt0L-high analysis and the full tt0L combination are presented separately in order to quantify the improvement of the tt0L-low channel to the tt0L search. As per design, the tt0L-low signal regions extend the sensitivity to low mass mediator models, with an improvement up to about 15% for scalar mediator particles.

In addition, the negative logarithmic profile likelihood ratios $-2\,\Delta\ln(\Lambda)(\mathcal{B}_{H\to\text{inv}};\theta)$ as a function of $\mathcal{B}_{H\to\text{inv}}$ for the tt0L-low and tt0L-high analyses, and their combination are illustrated in Figure 11. Table 6

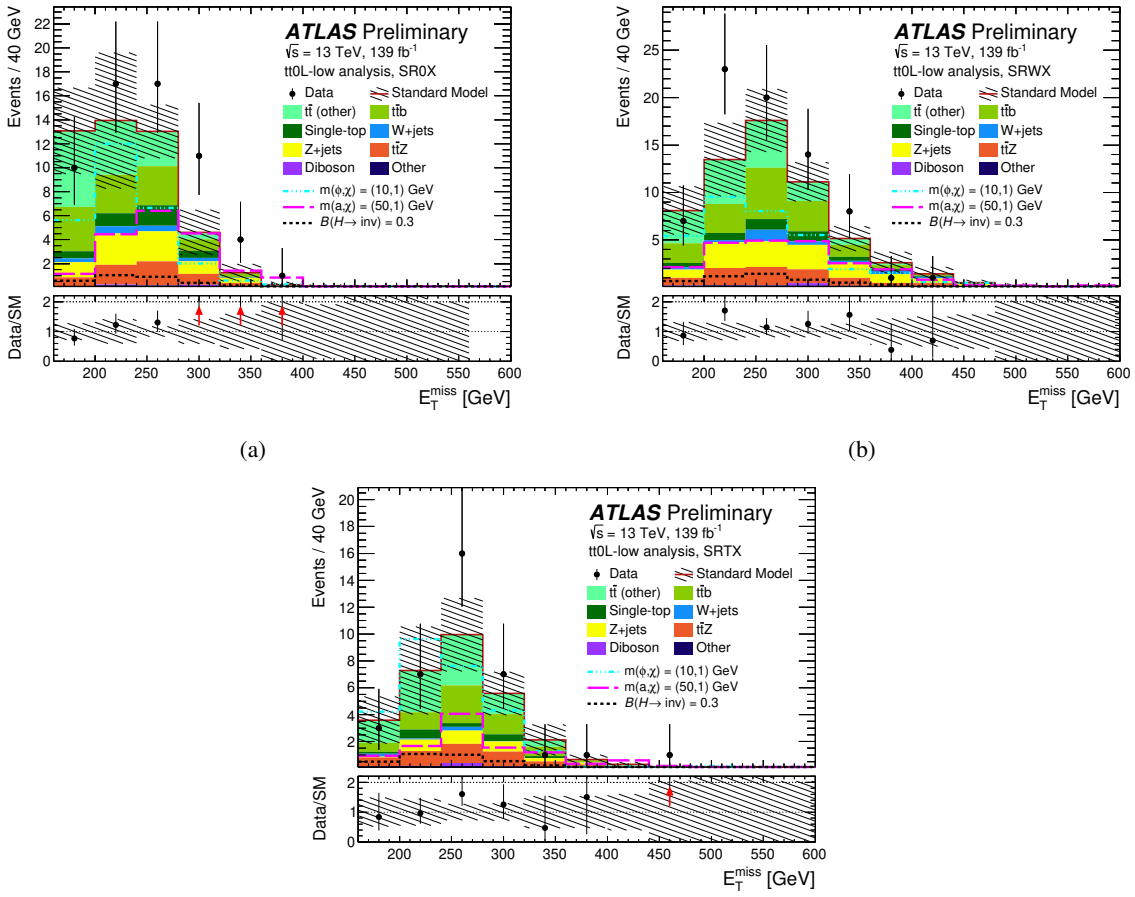

(a)

(b)

(c)

Figure 9: $E_{\mathrm{T}}^{\mathrm{miss}}$ distributions in (a) SR0X, (b) SRWX and (c) SRTX passing all the SR requirements. The contributions from all SM backgrounds are shown after the profile likelihood simultaneous fit to all tt0L-low CRs, with the hashed bands representing the total uncertainty. '$t\bar{t}$ (other)' represents $t\bar{t}$ events without extra jets or events with extra light flavour jets. 'Other' includes contributions from $t\bar{t}+W$, tZ and tWZ processes. The expected distributions for selected signal models are also shown as dashed lines. The overflow events are covered in the last bin. The bottom panels show the ratio of the observed data to the total SM background prediction, with the hatched area representing the total uncertainty in the background prediction and the red arrows marking data outside the vertical-axis range.

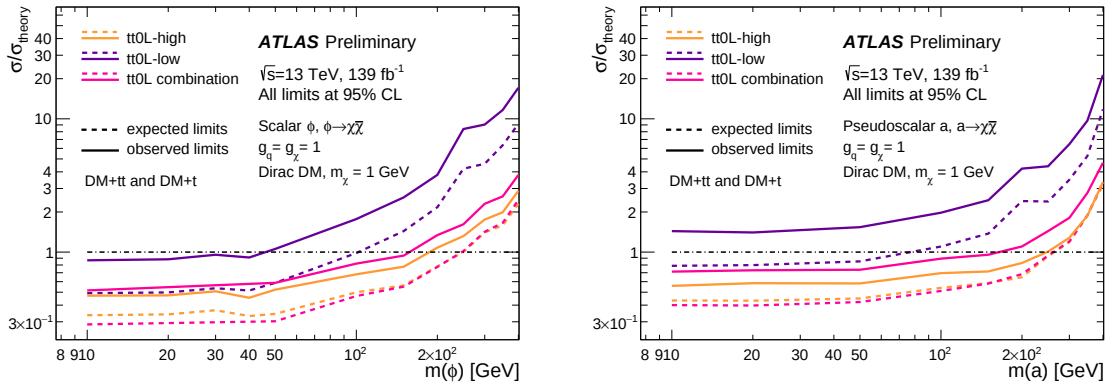

(a) (b)

Figure 10: Exclusion limits for colour-neutral (a) scalar or (b) pseudoscalar mediator dark matter models as a function of the mediator mass $m(\phi)$ or $m(a)$ for a DM mass $m_\chi = 1$ GeV. Associated production of DM with both single top quarks (tW and tj channels) and top quark pairs are considered. The limits are calculated at 95% CL and are expressed in terms of the ratio of the excluded cross section to the nominal cross section for a coupling assumption of $g = g_q = g_\chi = 1$. The solid (dashed) lines show the observed (expected) exclusion limits for the tt0L-high and tt0L-low analyses and their statistical combination.

presents the best-fit value, the observed and expected upper limits on $\mathcal{B}_{H\to\text{inv}}$ at the 95% CL for the tt0L-low analysis, the tt0L-high analysis and their statistical combination. As the tt0L-low selection was designed to target low mediator masses, the improvement in the expected upper limit at the Higgs boson mass is found to be relatively small.

Table 6: Results from the tt0L-low and tt0L-high searches for invisible decays of the 125 GeV Higgs boson in the $t\bar{t}H$ topology using 139 fb^{-1} of Run 2 data, and their statistical combination. Shown are the best-fit values of $\mathcal{B}_{H\to\text{inv}}$, as well as observed and expected upper limits on $\mathcal{B}_{H\to\text{inv}}$ at the 95% CL. The corresponding Asimov datasets for the expected results are constructed using nuisance parameter values from a fit to data with $\mathcal{B}_{H\to\text{inv}} = 0$, and the quoted uncertainty corresponds to the 68% confidence interval.

Analysis	Best fit $\mathcal{B}_{H\to\text{inv}}$	Observed upper limit	Expected upper limit	Reference
tt0L-low	$0.88^{+0.48}_{-0.46}$	1.80	$1.09^{+0.50}_{-0.26}$	this document
tt0L-high	$0.27^{+0.28}_{-0.27}$	0.80	$0.59^{+0.29}_{-0.18}$	[27], this document
tt0L comb.	$0.48^{+0.27}_{-0.27}$	0.95	$0.52^{+0.23}_{-0.16}$	[27], this document

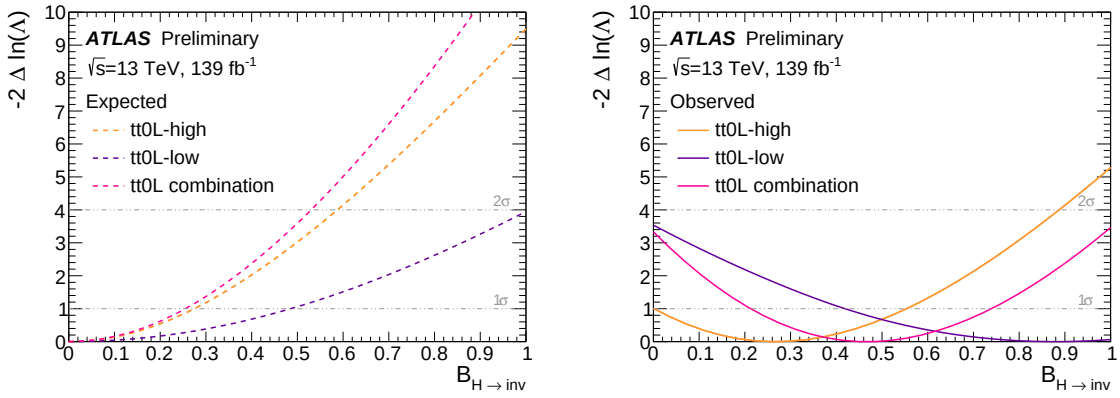

(a) (b)

Figure 11: (a) The expected negative logarithmic profile likelihood ratios $-2\,\Delta\ln(\Lambda)$ as a function of $\mathcal{B}_{H\to\text{inv}}$ for the each of the two tt0L analyses and their statistical combination. (b) Shown are the same distributions for the observed curves.

References

[1] F. Zwicky, *Die Rotverschiebung von extragalaktischen Nebeln*, Helv. Phys. Acta **6** (1933) 110 (cit. on p. 2).

[2] G. Bertone, D. Hooper and J. Silk, *Particle dark matter: Evidence, candidates and constraints*, Phys. Rept. **405** (2005) 279, arXiv: hep-ph/0404175 (cit. on p. 2).

[3] E. Komatsu et al., *Seven-Year Wilkinson Microwave Anisotropy Probe (WMAP) Observations: Cosmological Interpretation*, Astrophys. J. Suppl. **192** (2011) 18, arXiv: 1001.4538 [astro-ph.CO] (cit. on p. 2).

[4] P. A. R. Ade et al., *Planck 2015 results. XIII. Cosmological parameters*, Astron. Astrophys. **594** (2016) A13, arXiv: 1502.01589 [astro-ph.CO] (cit. on p. 2).

[5] G. Steigman and M. S. Turner, *Cosmological Constraints on the Properties of Weakly Interacting Massive Particles*, Nucl. Phys. B **253** (1985) 375 (cit. on p. 2).

[6] ATLAS Collaboration, *Search for new phenomena in events with an energetic jet and missing transverse momentum in pp collisions at $\sqrt{s}$ = 13 TeV with the ATLAS detector*, Phys. Rev. D **103** (2021) 112006, arXiv: 2102.10874 [hep-ex] (cit. on p. 2).

[7] CMS Collaboration, *Search for dark matter produced in association with a leptonically decaying Z boson in proton–proton collisions at $\sqrt{s}$ = 13 TeV*, Eur. Phys. J. C **81** (2021) 13, arXiv: 2008.04735 [hep-ex] (cit. on p. 2).

[8] ATLAS Collaboration, *Search for new phenomena in final states with b-jets and missing transverse momentum in $\sqrt{s}$ = 13 TeV pp collisions with the ATLAS detector*, JHEP **05** (2021) 093, arXiv: 2101.12527 [hep-ex] (cit. on p. 2).

[9] ATLAS Collaboration, *Search for dark matter in association with an energetic photon in pp collisions at $\sqrt{s}$ = 13 TeV with the ATLAS detector*, JHEP **02** (2021) 226, arXiv: 2011.05259 [hep-ex] (cit. on p. 2).

[10] ATLAS Collaboration, *Search for dark matter produced in association with bottom or top quarks in $\sqrt{s}$ = 13 TeV pp collisions with the ATLAS detector*, Eur. Phys. J. C **78** (2018) 18, arXiv: 1710.11412 [hep-ex] (cit. on p. 2).

[11] ATLAS Collaboration, *Search for dark matter produced in association with a Standard Model Higgs boson decaying into b-quarks using the full Run 2 dataset from the ATLAS detector*, JHEP **11** (2021) 209, arXiv: 2108.13391 [hep-ex] (cit. on p. 2).

[12] ATLAS Collaboration, *Constraints on mediator-based dark matter and scalar dark energy models using $\sqrt{s}$ = 13 TeV pp collision data collected by the ATLAS detector*, JHEP **05** (2019) 142, arXiv: 1903.01400 [hep-ex] (cit. on p. 2).

[13] A. Boveia et al., *Recommendations on presenting LHC searches for missing transverse energy signals using simplified s-channel models of dark matter*, Phys. Dark Univ. **27** (2020) 100365, ed. by O. Buchmueller et al., arXiv: 1603.04156 [hep-ex] (cit. on p. 2).

[14] A. Albert et al., *Recommendations of the LHC Dark Matter Working Group: Comparing LHC searches for dark matter mediators in visible and invisible decay channels and calculations of the thermal relic density*, Phys. Dark Univ. **26** (2019) 100377, arXiv: 1703.05703 [hep-ex] (cit. on p. 2).

[15] T. Abe et al., *LHC Dark Matter Working Group: Next-generation spin-0 dark matter models*, Phys. Dark Univ. **27** (2020) 100351, arXiv: 1810.09420 [hep-ex] (cit. on p. 2).

[16] D. Abercrombie et al., *Dark Matter benchmark models for early LHC Run-2 Searches: Report of the ATLAS/CMS Dark Matter Forum*, Phys. Dark Univ. **27** (2020) 100371, ed. by A. Boveia, C. Doglioni, S. Lowette, S. Malik and S. Mrenna, arXiv: 1507.00966 [hep-ex] (cit. on p. 2).

[17] M. Blanke, P. Pani, G. Polesello and G. Rovelli, *Single-top final states as a probe of top-flavoured dark matter models at the LHC*, JHEP **01** (2021) 194, arXiv: 2010.10530 [hep-ph] (cit. on p. 2).

[18] S. Westhoff, *New physics searches with top quarks*, PoS **LeptonPhoton2019** (2019) 012, arXiv: 1912.02054 [hep-ph] (cit. on p. 2).

[19] U. Haisch and G. Polesello, *Searching for production of dark matter in association with top quarks at the LHC*, JHEP **02** (2019) 029, arXiv: 1812.00694 [hep-ph] (cit. on p. 2).

[20] U. Haisch, P. Pani and G. Polesello, *Determining the CP nature of spin-0 mediators in associated production of dark matter and $t\bar{t}$ pairs*, JHEP **02** (2017) 131, arXiv: 1611.09841 [hep-ph] (cit. on pp. 2, 13).

[21] U. Haisch and E. Re, *Simplified dark matter top-quark interactions at the LHC*, JHEP **06** (2015) 078, arXiv: 1503.00691 [hep-ph] (cit. on p. 2).

[22] J. Abdallah et al., *Simplified Models for Dark Matter Searches at the LHC*, Phys. Dark Univ. **9-10** (2015) 8, arXiv: 1506.03116 [hep-ph] (cit. on p. 2).

[23] M. R. Buckley, D. Feld and D. Goncalves, *Scalar Simplified Models for Dark Matter*, Phys. Rev. **D 91** (2015) 015017, arXiv: 1410.6497 [hep-ph] (cit. on p. 2).

[24] G. D'Ambrosio, G. F. Giudice, G. Isidori and A. Strumia, *Minimal flavor violation: An Effective field theory approach*, Nucl. Phys. B **645** (2002) 155, arXiv: hep-ph/0207036 (cit. on p. 2).

[25] D. Pinna, A. Zucchetta, M. R. Buckley and F. Canelli, *Single top quarks and dark matter*, Phys. Rev. D **96** (2017) 035031, arXiv: 1701.05195 [hep-ph] (cit. on pp. 2, 14).

[26] P. Pani and G. Polesello, *Dark matter production in association with a single top-quark at the LHC in a two-Higgs-doublet model with a pseudoscalar mediator*, Phys. Dark Univ. **21** (2018) 8, arXiv: 1712.03874 [hep-ph] (cit. on p. 2).

[27] ATLAS Collaboration, *Search for a scalar partner of the top quark in the all-hadronic $t\bar{t}$ plus missing transverse momentum final state at $\sqrt{s} = 13$ TeV with the ATLAS detector*, Eur. Phys. J. C **80** (2020) 737, arXiv: 2004.14060 [hep-ex] (cit. on pp. 2, 3, 5, 6, 8, 11, 12, 15, 24).

[28] ATLAS Collaboration, *Search for new phenomena with top quark pairs in final states with one lepton, jets, and missing transverse momentum in pp collisions at $\sqrt{s} = 13$ TeV with the ATLAS detector*, JHEP **04** (2020) 174, arXiv: 2012.03799 [hep-ex] (cit. on pp. 2, 5, 11, 12, 15).

[29] ATLAS Collaboration, *Search for new phenomena in events with two opposite-charge leptons, jets and missing transverse momentum in pp collisions at $\sqrt{s} = 13$ TeV with the ATLAS detector*, JHEP **04** (2021) 165, arXiv: 2102.01444 [hep-ex] (cit. on pp. 2, 5, 11, 12, 15).

[30] ATLAS Collaboration, *The ATLAS Experiment at the CERN Large Hadron Collider*, JINST **3** (2008) S08003 (cit. on p. 3).

[31] ATLAS Collaboration, *Configuration and performance of the ATLAS b-jet triggers in Run 2*, Eur. Phys. J. C **81** (2021) 1087, arXiv: 2106.03584 [hep-ex] (cit. on pp. 3, 4).

[32] ATLAS Collaboration, *Search for dark matter produced in association with a single top quark in $\sqrt{s} = 13$ TeV pp collisions with the ATLAS detector*, Eur. Phys. J. C **81** (2021) 860, arXiv: 2011.09308 [hep-ex] (cit. on p. 3).

[33] ATLAS Collaboration, *Observation of a new particle in the search for the Standard Model Higgs boson with the ATLAS detector at the LHC*, Phys. Lett. B **716** (2012) 1, arXiv: 1207.7214 [hep-ex] (cit. on p. 3).

[34] D. de Florian et al., *Handbook of LHC Higgs Cross Sections: 4. Deciphering the Nature of the Higgs Sector*, **2/2017** (2016), arXiv: 1610.07922 [hep-ph] (cit. on pp. 3, 13).

[35] R. E. Shrock and M. Suzuki, *Invisible Decays of Higgs Bosons*, Phys. Lett. B **110** (1982) 250 (cit. on p. 3).

[36] D. Choudhury and D. P. Roy, *Signatures of an invisibly decaying Higgs particle at LHC*, Phys. Lett. B **322** (1994) 368, arXiv: hep-ph/9312347 [hep-ph] (cit. on p. 3).

[37] N. Arkani-Hamed, S. Dimopoulos, G. R. Dvali and J. March-Russell, *Neutrino masses from large extra dimensions*, Phys. Rev. D **65** (2001) 024032, arXiv: hep-ph/9811448 [hep-ph] (cit. on p. 3).

[38] O. J. P. Eboli and D. Zeppenfeld, *Observing an invisible Higgs boson*, Phys. Lett. B **495** (2000) 147, arXiv: hep-ph/0009158 [hep-ph] (cit. on p. 3).

[39] R. M. Godbole, M. Guchait, K. Mazumdar, S. Moretti and D. P. Roy, *Search for 'invisible' Higgs signals at LHC via associated production with gauge bosons*, Phys. Lett. B **571** (2003) 184, arXiv: hep-ph/0304137 [hep-ph] (cit. on p. 3).

[40] I. Antoniadis, M. Tuckmantel and F. Zwirner,
Phenomenology of a leptonic goldstino and invisible Higgs boson decays,
Nucl. Phys. B **707** (2005) 215, arXiv: hep-ph/0410165 [hep-ph] (cit. on p. 3).

[41] H. Davoudiasl, T. Han and H. E. Logan,
Discovering an invisibly decaying Higgs at hadron colliders, Phys. Rev. D **71** (2005) 115007,
arXiv: hep-ph/0412269 [hep-ph] (cit. on p. 3).

[42] B. Patt and F. Wilczek, *Higgs-field portal into hidden sectors*, (2006),
arXiv: hep-ph/0605188 [hep-ph] (cit. on p. 3).

[43] S. Kanemura, S. Matsumoto, T. Nabeshima and N. Okada,
Can WIMP Dark Matter overcome the Nightmare Scenario?, Phys. Rev. D **82** (2010) 055026,
arXiv: 1005.5651 [hep-ph] (cit. on p. 3).

[44] A. Djouadi, O. Lebedev, Y. Mambrini and J. Quevillon,
Implications of LHC searches for Higgs–portal dark matter, Phys. Lett. B **709** (2012) 65,
arXiv: 1112.3299 [hep-ph] (cit. on p. 3).

[45] D. Ghosh, R. Godbole, M. Guchait, K. Mohan and D. Sengupta,
Looking for an Invisible Higgs Signal at the LHC, Phys. Lett. B **725** (2013) 344,
arXiv: 1211.7015 [hep-ph] (cit. on p. 3).

[46] G. Belanger, B. Dumont, U. Ellwanger, J. F. Gunion and S. Kraml,
Status of invisible Higgs decays, Phys. Lett. B **723** (2013) 340, arXiv: 1302.5694 [hep-ph]
(cit. on p. 3).

[47] D. Curtin et al., *Exotic decays of the 125 GeV Higgs boson*, Phys. Rev. D **90** (2014) 075004,
arXiv: 1312.4992 [hep-ph] (cit. on p. 3).

[48] M. Zaazoua, L. Truong, K. A. Assamagan and F. Fassi, *Higgs portal vector dark matter interpretation: review of Effective Field Theory approach and ultraviolet complete models*, (2021),
arXiv: 2107.01252 [hep-ph] (cit. on p. 3).

[49] ATLAS Collaboration,
Combination of Searches for Invisible Higgs Boson Decays with the ATLAS Experiment,
Phys. Rev. Lett. **122** (2019) 231801, arXiv: 1904.05105 [hep-ex] (cit. on p. 3).

[50] CMS Collaboration, *Search for invisible decays of a Higgs boson produced through vector boson fusion in proton–proton collisions at* $\sqrt{s} = 13$ *TeV*, Phys. Lett. B **793** (2019) 520,
arXiv: 1809.05937 [hep-ex] (cit. on p. 3).

[51] ATLAS Collaboration, *Search for invisible Higgs-boson decays in events with vector-boson fusion signatures using 139* fb^{-1} *of proton-proton data recorded by the ATLAS experiment*, (2022),
arXiv: 2202.07953 [hep-ex] (cit. on p. 3).

[52] CMS Collaboration, *Search for invisible decays of the Higgs boson produced via vector boson fusion in proton-proton collisions at* $\sqrt{s} = 13$ *TeV*, (2022), arXiv: 2201.11585 [hep-ex]
(cit. on p. 3).

[53] ATLAS Collaboration, *The ATLAS Collaboration Software and Firmware*,
ATL-SOFT-PUB-2021-001, 2021, URL: https://cds.cern.ch/record/2767187
(cit. on p. 3).

[54] ATLAS Collaboration, *Vertex Reconstruction Performance of the ATLAS Detector at* $\sqrt{s} = 13$ *TeV*,
ATL-PHYS-PUB-2015-026, 2015, URL: https://cds.cern.ch/record/2037717
(cit. on p. 3).

[55] ATLAS Collaboration, *Electron and photon performance measurements with the ATLAS detector using the 2015–2017 LHC proton–proton collision data*, JINST **14** (2019) P12006, arXiv: 1908.00005 [hep-ex] (cit. on p. 3).

[56] ATLAS Collaboration, *Muon reconstruction performance of the ATLAS detector in proton–proton collision data at* $\sqrt{s} = 13$ *TeV*, Eur. Phys. J. C **76** (2016) 292, arXiv: 1603.05598 [hep-ex] (cit. on p. 3).

[57] ATLAS Collaboration, *Identification and energy calibration of hadronically decaying tau leptons with the ATLAS experiment in pp collisions at* $\sqrt{s} = 8$ *TeV*, Eur. Phys. J. C **75** (2015) 303, arXiv: 1412.7086 [hep-ex] (cit. on p. 3).

[58] M. Cacciari, G. P. Salam and G. Soyez, *The anti-k_t jet clustering algorithm*, JHEP **04** (2008) 063, arXiv: 0802.1189 [hep-ph] (cit. on p. 4).

[59] M. Cacciari, G. P. Salam and G. Soyez, *FastJet user manual*, Eur. Phys. J. C **72** (2012) 1896, arXiv: 1111.6097 [hep-ph] (cit. on p. 4).

[60] ATLAS Collaboration, *Performance of b-jet identification in the ATLAS experiment*, JINST **11** (2016) P04008, arXiv: 1512.01094 [hep-ex] (cit. on p. 4).

[61] ATLAS Collaboration, *Optimisation of the ATLAS b-tagging performance for the 2016 LHC Run*, ATL-PHYS-PUB-2016-012, 2016, URL: https://cds.cern.ch/record/2160731 (cit. on p. 4).

[62] ATLAS Collaboration, *Performance of missing transverse momentum reconstruction with the ATLAS detector using proton–proton collisions at* $\sqrt{s} = 13$ *TeV*, Eur. Phys. J. C **78** (2018) 903, arXiv: 1802.08168 [hep-ex] (cit. on p. 4).

[63] ATLAS Collaboration, *Performance of electron and photon triggers in ATLAS during LHC Run 2*, Eur. Phys. J. C **80** (2020) 47, arXiv: 1909.00761 [hep-ex] (cit. on p. 4).

[64] ATLAS Collaboration, *Performance of the ATLAS muon triggers in Run 2*, JINST **15** (2020) P09015, arXiv: 2004.13447 [hep-ex] (cit. on p. 4).

[65] ATLAS Collaboration, *Performance of the missing transverse momentum triggers for the ATLAS detector during Run-2 data taking*, JHEP **08** (2020) 080, arXiv: 2005.09554 [hep-ex] (cit. on p. 4).

[66] ATLAS Collaboration, *Luminosity determination in pp collisions at* $\sqrt{s} = 13$ *TeV using the ATLAS detector at the LHC*, ATLAS-CONF-2019-021, 2019, URL: https://cds.cern.ch/record/2677054 (cit. on p. 4).

[67] G. Avoni et al., *The new LUCID-2 detector for luminosity measurement and monitoring in ATLAS*, JINST **13** (2018) P07017 (cit. on p. 4).

[68] ATLAS Collaboration, *ATLAS data quality operations and performance for 2015–2018 data-taking*, JINST **15** (2020) P04003, arXiv: 1911.04632 [physics.ins-det] (cit. on p. 4).

[69] ATLAS Collaboration, *The ATLAS Simulation Infrastructure*, Eur. Phys. J. C **70** (2010) 823, arXiv: 1005.4568 [physics.ins-det] (cit. on pp. 4, 5).

[70] GEANT4 Collaboration, S. Agostinelli et al., *GEANT4 – a simulation toolkit*, Nucl. Instrum. Meth. A **506** (2003) 250 (cit. on pp. 4, 5).

[71] T. Sjöstrand et al., *An introduction to PYTHIA 8.2*, Comput. Phys. Commun. **191** (2015) 159, arXiv: 1410.3012 [hep-ph] (cit. on p. 4).

[72] T. Sjöstrand, S. Mrenna and P. Skands, *A brief introduction to PYTHIA 8.1*, Comput. Phys. Commun. **178** (2008) 852, arXiv: 0710.3820 [hep-ph] (cit. on p. 4).

[73] R. D. Ball et al., *Parton distributions with LHC data*, Nucl. Phys. B **867** (2013) 244, arXiv: 1207.1303 [hep-ph] (cit. on p. 4).

[74] ATLAS Collaboration, *The Pythia 8 A3 tune description of ATLAS minimum bias and inelastic measurements incorporating the Donnachie–Landshoff diffractive model*, ATL-PHYS-PUB-2016-017, 2016, URL: https://cds.cern.ch/record/2206965 (cit. on p. 4).

[75] S. Frixione, G. Ridolfi and P. Nason, *A positive-weight next-to-leading-order Monte Carlo for heavy flavour hadroproduction*, JHEP **09** (2007) 126, arXiv: 0707.3088 [hep-ph] (cit. on pp. 4, 5).

[76] P. Nason, *A new method for combining NLO QCD with shower Monte Carlo algorithms*, JHEP **11** (2004) 040, arXiv: hep-ph/0409146 (cit. on pp. 4, 5).

[77] S. Frixione, P. Nason and C. Oleari, *Matching NLO QCD computations with parton shower simulations: the POWHEG method*, JHEP **11** (2007) 070, arXiv: 0709.2092 [hep-ph] (cit. on pp. 4, 5).

[78] S. Alioli, P. Nason, C. Oleari and E. Re, *A general framework for implementing NLO calculations in shower Monte Carlo programs: the POWHEG BOX*, JHEP **06** (2010) 043, arXiv: 1002.2581 [hep-ph] (cit. on p. 4).

[79] M. Czakon and A. Mitov, *Top++: A program for the calculation of the top-pair cross-section at hadron colliders*, Comput. Phys. Commun. **185** (2014) 2930, arXiv: 1112.5675 [hep-ph] (cit. on p. 4).

[80] T. Gleisberg et al., *Event generation with SHERPA 1.1*, JHEP **02** (2009) 007, arXiv: 0811.4622 [hep-ph] (cit. on pp. 4, 5).

[81] T. Gleisberg and S. Höche, *Comix, a new matrix element generator*, JHEP **12** (2008) 039, arXiv: 0808.3674 [hep-ph] (cit. on pp. 4, 5).

[82] F. Cascioli, P. Maierhöfer and S. Pozzorini, *Scattering Amplitudes with Open Loops*, Phys. Rev. Lett. **108** (2012) 111601, arXiv: 1111.5206 [hep-ph] (cit. on pp. 4, 5).

[83] S. Schumann and F. Krauss, *A parton shower algorithm based on Catani–Seymour dipole factorisation*, JHEP **03** (2008) 038, arXiv: 0709.1027 [hep-ph] (cit. on pp. 4, 5).

[84] S. Höche, F. Krauss, M. Schönherr and F. Siegert, *QCD matrix elements + parton showers. The NLO case*, JHEP **04** (2013) 027, arXiv: 1207.5030 [hep-ph] (cit. on pp. 4, 5).

[85] S. Catani and M. Grazzini, *Next-to-Next-to-Leading-Order Subtraction Formalism in Hadron Collisions and its Application to Higgs-boson Production at the Large Hadron Collider*, Phys. Rev. Lett. **98** (2007) 222002, arXiv: hep-ph/0703012 [hep-ph] (cit. on p. 4).

[86] J. Alwall et al., *The automated computation of tree-level and next-to-leading order differential cross sections, and their matching to parton shower simulations*, JHEP **07** (2014) 079, arXiv: 1405.0301 [hep-ph] (cit. on p. 4).

[87] D. de Florian et al., *Handbook of LHC Higgs Cross Sections: 4. Deciphering the Nature of the Higgs Sector*, (2016), arXiv: 1610.07922 [hep-ph] (cit. on pp. 4, 5).

[88] L. Lönnblad, *Correcting the Colour-Dipole Cascade Model with Fixed Order Matrix Elements*, JHEP **05** (2002) 046, arXiv: hep-ph/0112284 (cit. on p. 4).

[89] R. D. Ball et al., *Parton distributions for the LHC run II*, JHEP **04** (2015) 040, arXiv: 1410.8849 [hep-ph] (cit. on pp. 4, 5).

[90] P. Artoisenet, R. Frederix, O. Mattelaer and R. Rietkerk, *Automatic spin-entangled decays of heavy resonances in Monte Carlo simulations*, JHEP **03** (2013) 015, arXiv: 1212.3460 [hep-ph] (cit. on p. 4).

[91] M. Backovic et al., *Higher-order QCD predictions for dark matter production at the LHC in simplified models with s-channel mediators*, Eur. Phys. J. C **75** (2015) 482, arXiv: 1508.05327 [hep-ph] (cit. on p. 4).

[92] H. B. Hartanto, B. Jäger, L. Reina and D. Wackeroth, *Higgs boson production in association with top quarks in the POWHEG BOX*, Phys. Rev. D **91** (2015) 094003, arXiv: 1501.04498 [hep-ph] (cit. on p. 5).

[93] D. J. Lange, *The EvtGen particle decay simulation package*, Nucl. Instrum. Meth. A **462** (2001) 152 (cit. on p. 5).

[94] ATLAS Collaboration, *ATLAS Pythia 8 tunes to 7 TeV data*, ATL-PHYS-PUB-2014-021, 2014, URL: https://cds.cern.ch/record/1966419 (cit. on p. 5).

[95] ATLAS Collaboration, *Object-based missing transverse momentum significance in the ATLAS Detector*, ATLAS-CONF-2018-038, 2018, URL: https://cds.cern.ch/record/2630948 (cit. on p. 5).

[96] M. Baak et al., *HistFitter software framework for statistical data analysis*, Eur. Phys. J. C **75** (2015) 153, arXiv: 1410.1280 [hep-ex] (cit. on p. 6).

[97] G. Cowan, K. Cranmer, E. Gross and O. Vitells, *Asymptotic formulae for likelihood-based tests of new physics*, Eur. Phys. J. C **71** (2011) 1554, arXiv: 1007.1727 [physics.data-an] (cit. on pp. 6, 12, 14), Erratum: Eur. Phys. J. C **73** (2013) 2501.

[98] T. Junk, *Confidence level computation for combining searches with small statistics*, Nucl. Instrum. Meth. A **434** (1999) 435, arXiv: hep-ex/9902006 (cit. on p. 6).

[99] A. L. Read, *Presentation of search results: the CL_S technique*, J. Phys. G **28** (2002) 2693 (cit. on p. 6).

[100] C. G. Lester and D. J. Summers, *Measuring masses of semiinvisibly decaying particles pair produced at hadron colliders*, Phys. Lett. B **463** (1999) 99, arXiv: hep-ph/9906349 (cit. on pp. 6, 11).

[101] A. Barr, C. Lester and P. Stephens, *m(T2): The Truth behind the glamour*, J. Phys. G **29** (2003) 2343, arXiv: hep-ph/0304226 (cit. on pp. 6, 11).

[102] ATLAS Collaboration, *Jet energy scale and resolution measured in proton–proton collisions at $\sqrt{s} = 13$ TeV with the ATLAS detector*, Eur. Phys. J. C **81** (2020) 689, arXiv: 2007.02645 [hep-ex] (cit. on p. 6).

[103] ATLAS Collaboration, *Formulae for Estimating Significance*, ATL-PHYS-PUB-2020-025, 2020, URL: https://cds.cern.ch/record/2736148 (cit. on p. 8).

[104] ATLAS Collaboration,
Search for top squark pair production in final states with one isolated lepton, jets, and missing transverse momentum in $\sqrt{s} = 8$ TeV pp collisions with the ATLAS detector, JHEP **11** (2014) 118, arXiv: 1407.0583 [hep-ex] (cit. on p. 10).

[105] ATLAS Collaboration,
Search for top-squark pair production in final states with one lepton, jets, and missing transverse momentum using $36\,fb^{-1}$ of $\sqrt{s} = 13$ TeV pp collision data with the ATLAS detector, JHEP **06** (2018) 108, arXiv: 1711.11520 [hep-ex] (cit. on p. 10).

[106] M. L. Graesser and J. Shelton, *Hunting Mixed Top Squark Decays*, Phys. Rev. Lett. **111** (2013) 121802, arXiv: 1212.4495 [hep-ph] (cit. on p. 11).

[107] W. Verkerke and D. P. Kirkby, *The RooFit toolkit for data modeling*, eConf **C0303241** (2003) MOLT007, arXiv: physics/0306116 [physics] (cit. on p. 12).

[108] L. Moneta et al., *The RooStats Project*, (2010), arXiv: 1009.1003 [physics.data-an] (cit. on p. 12).

[109] ATLAS Collaboration, *Constraints on new phenomena via Higgs boson couplings and invisible decays with the ATLAS detector*, JHEP **11** (2015) 206, arXiv: 1509.00672 [hep-ex] (cit. on pp. 12, 15).

[110] ATLAS Collaboration, *Calibration of the ATLAS b-tagging algorithm in $t\bar{t}$ semileptonic events*, ATLAS-CONF-2018-045, 2018, URL: https://cds.cern.ch/record/2638455 (cit. on p. 20).

[111] ATLAS Collaboration, *Search for heavy particles decaying into top-quark pairs using lepton-plus-jets events in proton–proton collisions at $\sqrt{s} = 13$ TeV with the ATLAS detector*, Eur. Phys. J. C **78** (2018) 565, arXiv: 1804.10823 [hep-ex] (cit. on p. 21).